RESEARCH ARTICLE

An estimation method for the fuel burn and other performance characteristics of civil transport aircraft; part 3 full flight profile when the trajectory is specified

D.I.A. Poll[1] and U. Schumann[2]

[1]Emeritus Professor of Aerospace Engineering, Cranfield University, Bedford, UK
[2]Deutsches Zentrum für Luft- und Raumfahrt, Institut für Physik der Atmosphäre, Oberpfaffenhofen, Germany
Corresponding author: D.I.A. Poll; Email: d.i.a.poll@cranfield.ac.uk

Abstract

If an aircraft's initial mass, the variation of true airspeed, true rate of climb, wind speed and wind direction with time and the relationship between barometric altitude and local temperature are known, the performance along the entire flight path can be determined. Previously published work has provided the building blocks for a simple, fast, open-source and transparent method to estimate the instantaneous fuel flow rate and the engine overall efficiency, plus several other performance characteristics for turbofan powered, civil transport aircraft. The flight phases of primary interest are the climb, cruise, descent and holding, when the flaps and undercarriage are fully retracted and the engine is providing significant, positive thrust. However, for completeness, an approximate relation is provided for the engine's 'flight idle' condition, together with simple estimates for fuel use during take-off and landing, plus a factor to allow for in-service deterioration. Detailed consideration is also given to the operating limits and relations are developed for the estimation of their location in Mach number and flight level space. To apply the method, a series of characteristic coefficients and constants must be known. Estimates for these quantities have been progressively improved and extended over time. Initially, results were published for 53 aircraft types and variants. The data base has now been extended to 67 entries and this is given in tabular form. Finally, to demonstrate the method's accuracy, estimates of fuel flow rate are compared with flight data recorder values for 20 complete flights of six different aircraft types.

Nomenclature

A_e	sum of the engine core and bypass jet exit cross sectional areas
AR	wing aspect ratio
a	constant in the skin friction law – Equation (33)
a_∞	speed of sound $= (\gamma \Re T_\infty)^{1/2}$
BPR	engine nominal bypass ratio
b	constant in the skin friction law – Equation (33)
b_f	fuselage width
Cd	airframe drag coefficient $= D/(q_\infty S_{ref})$
Cd_o	zero-lift drag coefficient
Cd_w	wave drag coefficient
C_L	overall lift coefficient $= L/(q_\infty S_{ref})$
C_F	mean skin friction coefficient – Equation (33)
C_P	specific heat at constant pressure for air
C_T	total aircraft net thrust coefficient $= n.F_n/(q_\infty S_{ref})$

C_t	engine net thrust coefficient $= F_n/(q_\infty A_e)$
$c_{1,2,3}$	dummy variables – Equations (E11), (E12) and (E13)
D	total drag force
e	aircraft Oswald efficiency factor
$FCOM$	flight crew operating manual
FL	flight level
F_n	net installed thrust per engine
g	acceleration due to gravity
g_n	net vertical acceleration due to gravity and Coriolis effect
g_{ISA}	acceleration due to gravity in the International standard atmosphere (9.80665m/sec^2 at sea level)
H	geopotential altitude above local sea level – Appendix A
h_{0-2}	engine dependent functions – Equations (24), (27) and (28)
h	geometric height above local sea level $=$ geodetic height
J_{1-3}	constants in Equations (42) and (44)
K s	lift-dependent drag factor – Equation (30)
k_1	miscellaneous lift-dependent drag factor – Equation (37)
L	lift force
LCV	lower calorific value of fuel ($\approx 43 \times 10^6 \text{J/kg}$ for kerosene)
L/D	lift-to-drag ratio
l	characteristic streamwise length $= S_{ref}^{1/2}$
M_∞	flight Mach number $= V_\infty /a_\infty$
M_{cc}	crest critical Mach number – Equation (40)
M_{TF}	'technology level' constant in Equation (41)
$MTOM$	maximum permitted take-off mass
m	instantaneous total aircraft mass
$\dot{m}_f$	fuel mass flow rate – summed over all engines
n	number of engines on aircraft
p	static pressure
p_i	impact pressure – Equation (59)
q_∞	freestream dynamic pressure $= 0.5\rho_\infty(V_\infty)^2 = 0.5\gamma p_\infty(M_\infty)^2$
R^{ac}	characteristic Reynolds number – Equation (34)
$\Re$	gas constant for air (287.05J/(kg K))
r	the geocentric radius of the Earth at sea level
r_E	equatorial radius
r_P	polar radius
S	distance travelled through the air
S_{ref}	aerodynamic reference wing area (Airbus definition)
s	wingspan
T	static temperature
T_R	engine throttle parameter – Equation (E4)
T_o	total temperature – Equation (E5)
$TCDS$	type certificate data sheet
TET	ratio of total temperature at turbine entry to freestream total temperature
t	time
V_G	speed along flight path relative to the ground
V_w	wind speed
V_∞	true air speed
X	wave drag variable – Equation (40)
β_h	aircraft heading angle
β_t	aircraft ground track angle
β_w	wind direction
γ	ratio of specific heats for air ($=1.4$)
δ_2	induced drag wing-fuselage interference factor
ε	angle between the thrust line and the flight direction
η_o	propulsion system overall efficiency – Equation (1)

η_2	constant in Equation (27)
θ	climb gradient – Equation (4)
Λ_w	wing quarter-chord sweep angle
μ	dynamic viscosity
ϕ	geocentric latitude
ρ	air density $= p/(\Re T)$
Σ	coefficient in Equation (24)
ψ_0, ψ_6	constant coefficients – Equations (32) and (49)
ω	Earth's angular velocity

Superscripts

ac	whole aircraft value

Subscripts

AC	at the aerodynamic ceiling
B	best, or local maximum, value
buff	at buffet onset
CAS	calibrated air speed
CO	crossover value
DO	at design optimum conditions
EAS	equivalent air speed
EC	engine characteristic value
FI	flight idle
IS	'in service' value
ISA	International Standard Atmosphere
LS	low speed
MU	maximum useable
MCC	maximum continuous climb rating
MTO	maximum take-off rating
MO	maximum permitted operational value
Max	maximum value
Min	minimum value
O	when $(\eta_o L/D)$ has its absolute maximum value
ref	reference
SC	at the service ceiling
SL	at sea level
SLS	at sea level static conditions
Stall	at the 1-g stall condition
TP	at the tropopause
ηB	when $(\eta_o L/D)$ has its best value at a given Mach number
∞	flight, or freestream, value

1.0 Introduction

Over the past 30 years, the atmospheric science community has been improving the understanding of the impact of global aviation on the environment. An essential element in this process has been the availability of performance estimates for individual aircraft. Until recently, attention has been focused on fuel use, since this determines the amounts of carbon dioxide, water vapour and NOx[1] that are released.

---

[1]The engine emits a mixture of nitric oxide and nitrogen dioxide, collectively refered to as NO_X.

However, it is now recognised that contrails and contrail induced cirrus cloud are an important contributor to climate change – see Schumann [1]. Prediction of contrail formation and its environmental impact requires a knowledge of the engine's overall efficiency, together with the number and physical characteristics of the non-volatile particulate matter (*nvPM*) in the exhaust. This places increased demands upon performance models and more comprehensive, more detailed and more accurate models are now required.

To address these challenges, a novel, open, transparent and independently verifiable performance model has been under development for several years, as reported in Poll [2] and Poll and Schumann [3, 4, 5, 6]. Currently, this provides estimates of fuel flow rate, thrust and engine overall efficiency for the cruise phase only, using a set of input parameters that characterise the airframe and engine combination. Estimates of these parameters have been published for 53 aircraft types – see Poll and Schumann [4, 5, 6]. However, since results are needed for all phases of flight, whilst the method is restricted to steady, straight and level flight, its usefulness is limited.

Here, an improved and extended version of the method is presented. This covers climb, cruise, initial descent and holding[2] for an aircraft in the clean configuration, i.e. with all high lift devices and the undercarriage fully retracted. In addition, a simple estimate is proposed for the engines in the flight idle condition sometimes employed during descent and, for completeness, first order estimates are provided for situations where the undercarriage and flaps are deployed, i.e. take-off, initial climb out, approach and landing.

For various reasons, large trajectory data sets may contain spurious, or erroneous information and consistency checks are needed so that potentially misleading data can be rejected. Therefore, detailed consideration is given to the aircraft operating envelope. Approximate relations are developed so that the permissible, or achievable, operational Mach number versus flight level (FL) space can be determined for an aircraft of given weight flying in a completely general atmosphere.

2.0 Extension to the general case

If the overall propulsive efficiency of the engine, η_o, is defined as

$$\eta_o = \frac{nF_nV_\infty}{\dot{m}_f LCV},$$

(1)

where n is the number of engines on the aircraft, F_n is the installed[3], net thrust per engine, V_∞ is the true airspeed, $\dot{m}_f$ is the total fuel mass flow rate and LCV is the lower[4] calorific value of the fuel, then the total fuel consumption per unit distance travelled through the air is

$$\frac{dm_f}{dS} = \frac{\dot{m}_f}{V_\infty} = -\frac{dm}{dS} = \left(\frac{nF_n}{D}\right)\left(\frac{L}{(\eta_o L/D)\,LCV}\right).$$

(2)

Here m is the instantaneous aircraft mass, S is the distance travelled through the air, L is the lift and D is the drag. In general, η_o depends upon the net thrust, the altitude and the Mach number, M_∞, whilst L/D depends upon the drag, the altitude and M_∞.

In the general flight situation, thrust is not equal to the drag and lift is not equal to the weight. Therefore, consider an aircraft accelerating and climbing in the vertical plane through still air with an instantaneous speed, V_∞, relative to a stationary, ground-based observer, as shown in Fig. 1. In general, the engine thrust line is set at a fixed angle, known as the thrust setting angle, relative to the aircraft's longitudinal datum. Hence, the angle, ε, between the thrust line and the direction of travel

---

[2]It should be noted that not all holding takes place in the clean condition.

[3]An engine installed in an aircraft delivers about 97% of the thrust of the same engine in isolation, e.g. on a test bed.

[4]The lower value is appropriate since water generated in the combustion process leaves the engine in its gaseous phase.
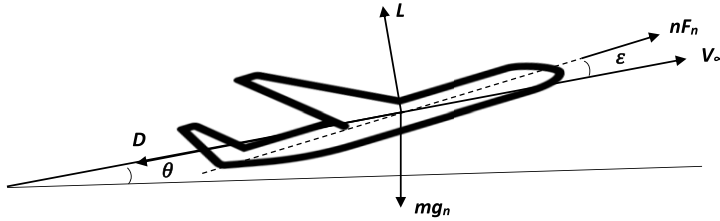
Figure 1. *The forces acting upon an aircraft accelerating and climbing in the vertical plane through still air.*

is equal to the sum of the thrust setting angle and the angle-of-attack, also measured relative to the aircraft's longitudinal datum. Since the air is still, V_∞ is also equal to the airspeed and the ground speed, V_G, is

$$V_G = \frac{V_\infty}{\cos\theta}, \tag{3}$$

where θ is the climb gradient and, if h is the geometric height above local sea level[5], then

$$\sin\theta = \frac{dh/dt}{V_\infty} \text{ and } \cos\theta = \left(1 - \left(\frac{dh/dt}{V_\infty}\right)^2\right)^{1/2}. \tag{4}$$

Relative to the ground-based frame of reference, when an aircraft is following a curved path in the vertical plane, whilst losing mass as fuel is consumed, the acceleration along the flight path is

$$\frac{1}{g_n}\frac{dV_\infty}{dt} = \left(\frac{n.F_n\cos\varepsilon - D}{mg_n}\right) - \sin\theta + \frac{V_\infty \dot{m}_f}{g_n m} \tag{5}$$

and the acceleration normal to the flight path is

$$\frac{V_\infty}{g_n}\frac{d\theta}{dt} = \left(\frac{L + n.F_n\sin\varepsilon}{mg_n}\right) - \cos\theta \approx 0, \tag{6}$$

see for example Bower et al. [7].

    Strictly speaking, since the Earth is rotating, a co-ordinate system fixed to the ground is not an inertial frame of reference. Consequently, the quantity g_n includes not only the planet's gravitational acceleration, g, but also the vertical component of the Coriolis acceleration and the centrifugal acceleration due to the aircraft's speed relative to the ground. As shown in Appendix A, g is the sum of Newtonian gravity and the vertical component of the Earth's centrifugal acceleration. Both these elements are functions of latitude, ϕ and h. On the other hand, the vertical component of the Coriolis acceleration depends upon ϕ, V_G, and aircraft's ground track relative to true North, β_t, – see, for example, Menke and Abbott [8]. In addition, since an aircraft flying at fixed height is also following a circular path, V_G provides an additional centrifugal acceleration. Combining the two effects gives

$$g_n - g = -2\omega V_G\sin\beta_t\cos\phi - \frac{V_G^2}{(r+h)}, \tag{7}$$

where r is the Earth's geocentric radius at sea level and ω is Earth's angular velocity. This acceleration component is sometimes referred to as the "Eötvös[6] effect".

    For civil transport aircraft, ε is usually less than 5 degrees and so its influence is always small. In addition, the climb gradient, θ, is typically less than 10 degrees and, to ensure passenger comfort, accelerations normal to the flight path are maintained at low levels. Consequently, θ is always a relatively

---

[5]Since the Earth is approximately ellipsoidal, this is the geodetic height.
[6]A Hungarian name pronounced "Urtvesh".

small angle and any acceleration normal to the flight path can be neglected without causing a significant loss of accuracy.

Therefore, if the instantaneous mass of the aircraft, true airspeed, rate of climb, acceleration along the flight path and lift-to-drag ratio are known, the total required thrust is given by

$$\frac{n.F_n}{m(g_{SL})_{ISA}} = \left(\frac{g_n}{(g_{SL})_{ISA}}\right)\left(\left(\frac{\cos\theta}{L/D}\right) + \sin\theta\right) + \frac{1}{(g_{SL})_{ISA}}\left(\frac{dV_\infty}{dt} - V_\infty\frac{\dot{m}_f}{m}\right), \tag{8}$$

whilst the required lift is

$$\frac{L}{m(g_{SL})_{ISA}} \approx \left(\frac{g_n}{(g_{SL})_{ISA}}\right)\cos\theta. \tag{9}$$

Here, $(g_{SL})_{ISA}$ is the (constant) reference value for gravity at sea level in the International Standard Atmosphere (*ISA*) [9].

As shown in Appendix A, relative to $(g_{SL})_{ISA}$, the maximum possible variation of g due to latitude changes is $\pm 0.25\%$, whilst, in current operations, the maximum variation of g relative to its value at sea level due to altitude changes is about -0.5%. Hence, at the global level, deviations in g from $(g_{SL})_{ISA}$ fall in the range $+0.25\%$ (sea level at the poles) to -0.75% (15,000m altitude at the equator). By comparison, the vertical component of the Coriolis acceleration has values in the range ± 0.035[7] m/s^2 (maximum at the equator), i.e. $\pm0.35\%$ of $(g_{SL})_{ISA}$, whilst the maximum centrifugal acceleration due to flight speed is about -0.01m/s^2, or -0.10% of $(g_{SL})_{ISA}$. Therefore, taking g_n to be equal to $(g_{SL})_{ISA}$, as is often the case in analytic work, introduces an error somewhere in the range $+0.5\%$ to -1.2%.

In general, the air through which the aircraft is travelling will not be still, i.e. there will be a wind. However, if the wind is horizontal with speed, V_w, and direction, β_w, measured relative to true North, and both quantities are steady, then according to Galileo's principle of independence, a frame of reference that moves with the air mass, i.e. with speed, V_w, and direction, β_w, relative to the ground, is also inertial. Relative to this 'wind fixed' frame of reference, V_∞ is still the airspeed, h is still the geometric height above local sea level and g is unchanged. However, the very small Eötvös acceleration in Equation (7) must always be evaluated relative to ground fixed axes and, if the aircraft heading is β_h, V_G and β_t are obtained from a solution of the vector wind triangle, see, for example, Huang and Cummings [10], i.e.

$$V_G = \sqrt{\left(\frac{V_\infty}{\cos\theta}\right)^2 + V_w^2 - 2\left(\frac{V_\infty V_w}{\cos\theta}\right)\cos(\beta_h - \beta_w)} \tag{10}$$

and

$$\beta_t = \beta_h + \sin^{-1}\left(\frac{V_w}{V_G}\sin(\beta_h - \beta_w)\right). \tag{11}$$

Consequently, subject only to this small correction, Equations (8) and (9) are valid for a steady, uniform wind. Nevertheless, during normal operations, significant wind velocity variations are to be expected, in which case, a frame of reference moving with the wind speed will no longer be inertial. However, if the horizontal wind has a component in the aircraft's direction of travel, i.e. a tail wind, V_{tw}, where

$$V_{tw} = -V_w\cos(\beta_h - \beta_w), \tag{12}$$

by analogy with the Coriolis acceleration, Equation (8) can be extended to include time varying, wind strength by the introduction of an additional, inertial force, i.e.

$$\begin{aligned}\frac{n.F_n}{m(g_{SL})_{ISA}} &= \left(\frac{g_n}{(g_{SL})_{ISA}}\right)\left(\left(\frac{\cos\theta}{L/D}\right) + \sin\theta\right) + \frac{1}{(g_{SL})_{ISA}}\left(\frac{dV_\infty}{dt} - V_\infty\frac{\dot{m}_f}{m}\right) \\ &+ \frac{\cos\theta}{(g_{SL})_{ISA}}\left(\frac{dV_{tw}}{dt} - V_{tw}\frac{\dot{m}_f}{m}\right).\end{aligned} \tag{13}$$

---

[7]Assuming flight in the *ISA* at the equator, travelling either due east, or due west, at 36,000 feet and with a Mach number 0.85.

As described in Appendix B, the aircraft's air data system uses impact pressure, p_i, measured with a Pitot tube, the local static pressure, p_∞, and total temperature, $(T_0)_\infty$ to determine the flight Mach number, M_∞, local static temperature, T_∞, and, hence, true airspeed, V_∞. However, whilst, as shown in Appendix A, the true rate of climb, dh/dt, can be obtained from a knowledge of the variation of p_∞ and T_∞ with time, the air data system alone cannot provide a value for h. Consequently, in operations, when an aircraft is above the 'transition' altitude,[8] h is replaced by the non-dimensional flight level, FL. By international agreement, using p_∞ from the air data system, FL is defined as the geopotential altitude, H, measured in feet, that the aircraft would have if it was operating in the International Standard Atmosphere [9] divided by 100. The relationship between flight level and p_∞ is also given in Appendix A.

When the trajectory is obtained from a ground-based source, e.g. an air navigation service provider, the information might be presented as values of ground speed, ground track and flight level at a series of waypoints. In this situation, again using the wind triangle, the airspeed is given by

$$V_\infty \cos \theta = \left(V_G^2 + V_w^2 + 2 V_G V_w \cos \left(\beta_t - \beta_w \right) \right)^{1/2}, \tag{14}$$

whilst, as shown in Appendix A, the true rate of climb is given by

$$\frac{1}{(a_{SL})_{ISA}} \frac{dh}{dt} = 0.08957 \left(\frac{(g_{SL})_{ISA}}{g} \right) \left(\frac{T_\infty}{(T_\infty)_{ISA}} \right) \frac{dFL}{dt} \quad \text{(m/s)}. \tag{15}$$

Here wind speed, wind direction and temperature information would have to be obtained from a meteorological service provider.

If the aircraft lift and drag coefficients have their usual definitions, i.e.

$$C_L = \frac{L}{(\gamma/2)\, p_\infty M_\infty^2 S_{ref}} \text{ and } C_D = \frac{D}{(\gamma/2)\, p_\infty M_\infty^2 S_{ref}}, \tag{16}$$

where air is taken to be an ideal gas, S_{ref} is the reference wing area, γ is the ratio of specific heats, plus a total thrust coefficient, C_T, defined as

$$C_T = \frac{n.F_n}{(\gamma/2)\, p_\infty M_\infty^2 S_{ref}}. \tag{17}$$

Then Equation (8) becomes

$$C_T = C_L \left(\frac{1}{L/D} + \tan\theta \right) + \frac{C_L}{\cos\theta} \left(\frac{(g_{SL})_{ISA}}{g_n} \right) \left(\frac{1}{(g_{SL})_{ISA}} \left(\frac{dV_\infty}{dt} - V_\infty \frac{\dot{m}_f}{m} \right) + \right.$$
$$\left. \frac{\cos\theta}{(g_{SL})_{ISA}} \left(\frac{dV_{tw}}{dt} - V_{tw} \frac{\dot{m}_f}{m} \right) \right). \tag{18}$$

This result is applicable to all phases of flight. Consequently, the total fuel consumed per unit time, $\dot{m}_f$, is given by combining Equations (1) and (18), i.e.

$$\dot{m}_f = \frac{n F_n V_\infty}{\eta_o LCV} = \left(\frac{\gamma}{2} \right) \left(\frac{C_T}{\eta_o} M_\infty^3 \right) \left(\frac{p_\infty a_\infty S_{ref}}{LCV} \right). \tag{19}$$

Further information on aircraft performance can be found in standard texts, e.g. Shevell [11] or Young [12].

3.0 Estimating the overall engine propulsive efficiency

The model relating engine overall efficieny to net thrust, altitiude and Mach number has been fully described in Poll and Schumann [6]. Therefore, only a summary will be presented here.

---

[8]The transition altitude is determined by the air traffic controller and it can range form 3,000 to 18,000 feet, depending upon conditions. Below this level, pressure height is measured relative to sea level, i.e. the altimeter reference value is local static pressure at sea level. Above it, the reference pressure is set to 1,013.25hPa, i.e. sea-level static in the *ISA*, and flight levels are used.
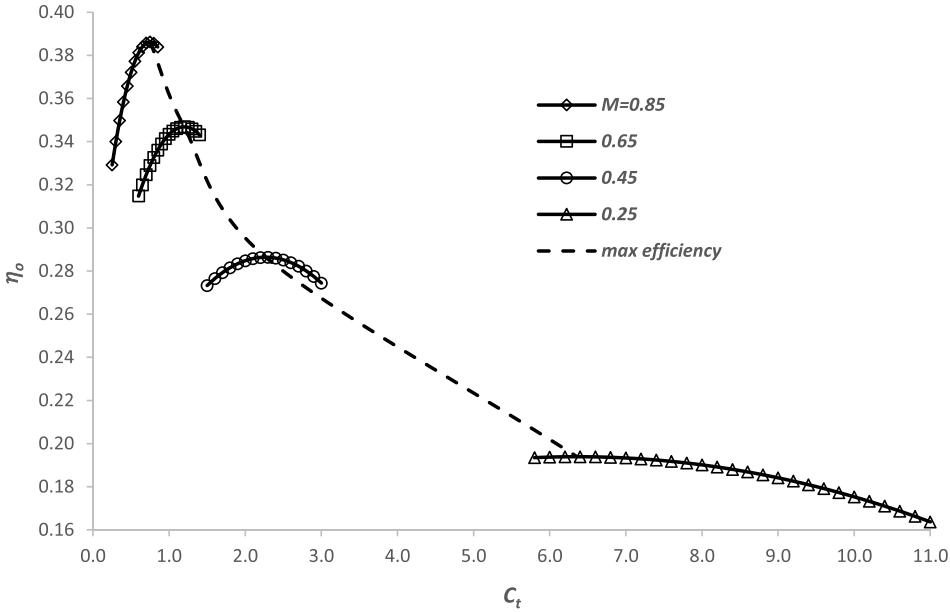
Figure 2. *The variation of overall efficiency with thrust coefficient and Mach number for a civil aircraft turbofan engine with a nominal bypass ratio of 8. Figure taken from Poll and Schumann [6].*

The thrust coefficient for an individual engine is given by

$$C_t = \frac{F_n}{(\gamma/2)\, p_\infty M_\infty^2 A_e}. \tag{20}$$

If the bypass and core flows are mixed at exit, A_e is the jet exit area. However, if the bypass and core flows are separate, A_e is the sum of the engine core and bypass jet exit cross sectional areas. Hence, from Equation (17), the total thrust coefficent is

$$C_T = \left(\frac{n.A_e}{S_{ref}}\right) C_t. \tag{21}$$

The typical variation of η_o with C_t and M_∞ is shown in Fig. 2. For operation at fixed Mach number, η_o goes though a local maximum, $(\eta_o)_B$, at a particular value of C_t, i.e. $(C_t)_{\eta B}$, and the locus of these 'best' points is given by the dashed line in Fig. 2. Poll and Schumann [6] have shown that, for a given Mach number, if the values of η_o are normalised with $(\eta_o)_B$ and the corresponding values of C_t are normalised with $(C_t)_{\eta B}$, the resulting curves are approximately independent of Mach number for Mach numbers greater than 0.4 and almost the same for all engines, irrespective of the overall pressure and bypass ratios.

Furthermore, since, from Equations (20) and (21),

$$\frac{C_t}{(C_t)_{\eta B}} = \frac{C_T}{(C_T)_{\eta B}}, \tag{22}$$

this near-universal curve for individual engines is also applicable to the complete aircraft and, for

$$0.3 \leq \frac{C_T}{(C_T)_{\eta B}} < 1.8, \tag{23}$$

it may be represented to a good approximation, by

$$\frac{\eta_o}{(\eta_o)_B} = h_0 \approx \left(1 - 0.43\left(\frac{C_T}{(C_T)_{\eta B}} - 1\right)^2\right)\left(1 + \Sigma\left(\frac{C_T}{(C_T)_{\eta B}} - 1\right)^2\right). \tag{24}$$

For M_∞ greater than 0.4, Σ is zero and, for

$$0.2 \leq M_\infty \leq 0.4, \tag{25}$$

$$\Sigma \approx 1.30 \left(0.4 - M_\infty\right). \tag{26}$$

If values of normalised overall efficiency are required for normalised thrust coefficients below 0.3, the variation may be represented by a fourth order polynomial as described in Appendix C.

In addition, it has been shown that $(\eta_o)_B$ and $(C_T)_{\eta B}$ are functions of the Mach number, such that, for Mach numbers greater than about 0.2,

$$\frac{(\eta_o)_B}{(\eta_o)_{DO}} = h_1 \approx \left(\frac{M_\infty}{M_{DO}}\right)^{\eta_2} \tag{27}$$

and

$$\frac{(C_t)_{\eta B}}{(C_t)_{DO}} = \frac{(C_T)_{\eta B}}{(C_T)_{DO}} = h_2 \approx \left(\frac{1 + 0.55 M_\infty}{1 + 0.55 M_{DO}}\right)\left(\frac{M_{DO}}{M_\infty}\right)^2. \tag{28}$$

Here, η_2 is a function of the bypass ratio, with

$$\eta_2 \approx 0.65 \left(1 - 0.035 \left(BPR\right)\right) \tag{29}$$

and $(\eta_o)_{DO}$, M_{DO}, and $(C_T)_{DO}$ are the 'design optimum' values.

The design optimum condition is the single combination of aircraft weight, flight level and Mach number at which both the airframe lift-to-drag ratio and the engine's overall efficiency have local maximum values when operating in a specified atmosphere, i.e. $(\eta_o \, L/D)$ is an absolute maximum. As described in Poll and Schumann [5], the design weight is set to 80% of the maximum permitted take-off value, i.e. a value close to a typical mid-cruise condition, and the design atmosphere is taken to be the International Standard Atmosphere [9]. The design optimum values are characteristic of the aircraft and engine combination. Therefore, when the $(\eta_o)_{DO}$, M_{DO}, and $(C_T)_{DO}$, are known, the normalising values $(\eta_o)_B$ and $(C_T)_{\eta B}$ for any other operating condition are obtained from Equations (27) and (28). These are then used in Equation (24) to give the corresponding value of η_o.

Estimates of $(\eta_o)_{DO}$, M_{DO}, and $(C_T)_{DO}$ for 53 different aircraft types and variants have been reported previously by Poll and Schumann [4, 5, 6]. This list has now been extended to cover 67 aircraft and the complete set of values can be found in Tables 1 and 2.

4.0 Estimating the lift-to-drag ratio for the clean configuration

The variation of an aircraft's drag with lift is known as its drag polar. During the take-off, very early climb, final approach and landing, the high lift devices are deployed and the undercarriage is lowered. However, above about 3,000 feet, the aircraft is usually in the clean condition with high lift devices and undercarriage fully retracted, but still travelling at low Mach number ($M_\infty < 0.6$). In this situation, when the lift coefficient lies between 0.3 to 0.7, the polar may be represented, approximately, by the classical two-term, low-speed form, i.e.

$$Cd = function \ (C_L, R^{ac}) \approx Cd_0 + \frac{C_L^2}{\pi . AR . e_{LS}} = Cd_0 + KC_L^2. \tag{30}$$

Here, K is the lift-dependent drag factor, AR is the wing aspect ratio, defined as

$$AR = \frac{s^2}{S_{ref}}, \tag{31}$$

Table 1. *Principal characteristics of a range of turbofan engines powering civil transport aircraft. The characteristics are averages over all engines appropriate to the aircraft type and the static thrust and fuel flow at flight idle are total aircraft values*

ICAO	First Flight	Nominal OPR	Nominal BPR	$(F_{00})_{ISA}$ (kN)	$(\dot{m}_f)_{max\ T/O}$ (kg/s)	$((\dot{m}_f)_{SLS})_{FI}$	M_{EC}	TR_{EC}	$(\eta_o)_{DO}$	η_1	$(C_T)_{DO}$	$(TET)_{MCC}$ (K)
A30B	1973	26	4.6	466	4.80	0.40	0.674	4.93	0.276	0.322	0.0350	1350
A306	1983	32	4.9	525	5.08	0.42	0.683	5.34	0.313	0.364	0.0307	1486
A310	1982	26	5.0	444	4.29	0.38	0.686	5.37	0.334	0.384	0.0329	1474
A313	1982	28	5.0	480	4.51	0.39	0.684	5.36	0.327	0.375	0.0329	1474
A318	2002	25	5.2	199	2.06	0.21	0.689	6.03	0.293	0.340	0.0309	1649
A319	1995	25	5.6	212	1.99	0.21	0.701	5.85	0.283	0.328	0.0316	1600
A320	1987	27	5.6	225	2.15	0.22	0.701	5.59	0.309	0.358	0.0347	1529
A321	1993	31	5.3	269	2.69	0.25	0.694	5.74	0.295	0.343	0.0359	1584
A332	1992	34	5.1	609	5.94	0.49	0.686	5.73	0.325	0.370	0.0250	1576
A333	1992	34	5.1	604	5.84	0.49	0.687	5.73	0.344	0.391	0.0258	1576
A338	2018	45	9.0	656	4.96	0.48	0.763	6.25	0.360	0.400	0.0229	1726
A339	2017	45	9.0	656	4.96	0.48	0.763	6.23	0.359	0.400	0.0239	1723
A342	1991	30	6.7	579	5.52	0.48	0.725	5.64	0.326	0.367	0.0268	1567
A343	1991	30	6.7	579	5.52	0.48	0.725	5.66	0.331	0.373	0.0281	1567
A345	2002	36	7.5	1036	8.79	0.92	0.740	5.67	0.324	0.362	0.0245	1649
A346	2001	37	7.5	1051	8.96	0.92	0.740	5.68	0.336	0.375	0.0258	1643
A359	2013	41	9.0	758	5.64	0.58	0.764	6.12	0.371	0.405	0.0225	1706
A35K	2016	49	8.0	873	7.01	0.65	0.749	6.17	0.364	0.400	0.0223	1719
A388	2005	38	7.9	1351	10.57	1.07	0.747	5.87	0.363	0.399	0.0216	1667
BCS1	2013	36	11.3	201	1.44	0.15	0.785	6.23	0.326	0.365	0.0304	1706
BCS3	2015	36	11.3	201	1.44	0.15	0.785	6.26	0.327	0.365	0.0316	1715
A20N	2014	34	11.6	256	1.77	0.18	0.787	6.25	0.326	0.363	0.0302	1711
A21N	2016	34	11.6	256	1.77	0.18	0.787	6.20	0.340	0.380	0.0328	1719
B712	1998	30	4.6	179	1.82	0.20	0.675	6.00	0.289	0.351	0.0376	1622
B722	1967	17	1.0	204	3.41	0.42	0.557	4.63	0.243	0.286	0.0328	1244
B732	1967	17	1.0	137	2.30	0.28	0.557	4.66	0.215	0.269	0.0359	1244
B733	1984	23	5.1	187	2.01	0.23	0.688	5.50	0.273	0.323	0.0384	1497
B734	1988	24	5.1	190	2.05	0.24	0.688	5.59	0.269	0.319	0.0377	1539

Table 1. *Continued.*

ICAO	First Flight	Nominal OPR	Nominal BPR	$(F_{00})_{ISA}$ (kN)	$(\dot{m}_f)_{max\ T/O}$ (kg/s)	$((\dot{m}_f)_{SLS})_{FI}$	M_{EC}	TR_{EC}	$(\eta_o)_{DO}$	η_1	$(C_T)_{DO}$	$(TET)_{MCC}$ (K)
B735	1989	23	5.1	187	2.01	0.23	0.688	5.69	0.255	0.302	0.0346	1549
B736	1997	23	5.4	190	1.88	0.20	0.695	5.90	0.289	0.335	0.0310	1615
B737	1997	26	5.2	214	2.18	0.21	0.691	5.90	0.279	0.323	0.0315	1615
B738	1997	28	5.1	233	2.43	0.22	0.688	5.90	0.287	0.333	0.0335	1615
B739	2006	28	5.1	233	2.43	0.22	0.688	6.10	0.282	0.327	0.0330	1672
B37M	2018	40	8.4	248	2.00	0.19	0.755	6.28	0.336	0.380	0.0305	1726
B38M	2016	40	8.4	248	2.00	0.19	0.755	6.26	0.338	0.383	0.0316	1719
B39M	2017	40	8.4	248	2.00	0.19	0.755	6.24	0.345	0.390	0.0331	1723
B742	1971	25	4.8	882	9.11	0.90	0.679	4.61	0.302	0.338	0.0259	1317
B743	1980	26	4.8	899	9.19	0.91	0.679	5.05	0.301	0.337	0.0253	1449
B744	1985	31	5.0	1021	9.79	0.82	0.684	5.30	0.318	0.356	0.0245	1508
B748	2010	43	8.0	1199	9.81	0.87	0.749	5.89	0.362	0.395	0.0224	1693
B752	1982	27	4.7	358	3.64	0.35	0.678	5.38	0.302	0.347	0.0280	1474
B753	1998	27	4.7	358	3.64	0.35	0.678	5.88	0.309	0.355	0.0306	1622
B762	1984	30	4.9	504	4.86	0.41	0.683	5.41	0.320	0.368	0.0272	1497
B763	1986	30	4.9	504	4.86	0.41	0.683	5.54	0.307	0.353	0.0240	1519
B764	1999	31	5.1	513	4.86	0.40	0.688	5.83	0.315	0.361	0.0278	1629
B77L	2005	41	7.2	1007	9.01	0.75	0.735	5.82	0.349	0.386	0.0239	1667
B772	1994	38	7.0	781	6.89	0.57	0.731	5.72	0.331	0.367	0.0242	1592
B77W	1994	42	7.1	1028	9.38	0.76	0.732	5.59	0.351	0.389	0.0264	1592
B773	1997	36	6.3	745	6.87	0.56	0.716	5.80	0.354	0.394	0.0266	1615
B788	2009	43	9.0	633	4.82	0.45	0.764	6.06	0.376	0.412	0.0238	1688
B789	2013	43	9.0	633	4.82	0.45	0.764	6.13	0.376	0.412	0.0239	1706
B78X	2017	46	8.9	689	5.33	0.47	0.762	6.19	0.365	0.400	0.0243	1723
E75S	2002	23	5.1	120	1.32	0.13	0.688	6.06	0.241	0.284	0.0339	1649
E75L	2002	23	5.1	120	1.32	0.13	0.688	6.06	0.241	0.284	0.0345	1649
E135	1995	17	4.8	66	0.72	0.09	0.680	5.92	0.226	0.273	0.0370	1600
E145	1995	19	4.7	74	0.82	0.10	0.678	5.92	0.242	0.292	0.0382	1600
E170	2002	23	5.1	120	1.32	0.13	0.688	6.06	0.241	0.284	0.0354	1649

Table 1. *Continued.*

ICAO	First Flight	Nominal OPR	Nominal BPR	$(F_{00})_{ISA}$ (kN)	$(\dot{m}_f)_{max\ T/O}$ (kg/s)	$((\dot{m}_f)_{SLS})_{FI}$	M_{EC}	TR_{EC}	$(\eta_o)_{DO}$	η_1	$(C_T)_{DO}$	$(TET)_{MCC}$ (K)
E190	2004	27	5.1	167	1.74	0.18	0.687	6.07	0.267	0.310	0.0338	1661
E195	2004	27	5.1	162	1.67	0.17	0.687	6.07	0.268	0.310	0.0349	1661
E290	2016	33	11.6	186	1.30	0.14	0.787	6.27	0.331	0.368	0.0292	1719
E295	2017	36	11.4	201	1.42	0.14	0.786	6.28	0.323	0.360	0.0312	1723
MD82	1981	20	1.7	185	2.62	0.27	0.583	5.44	0.245	0.299	0.0376	1462
MD83	1984	20	1.7	193	2.71	0.27	0.582	5.57	0.238	0.290	0.0379	1497
GLF5	1995	25	4.1	138	1.49	0.17	0.659	5.85	0.318	0.367	0.0293	1600
CRJ9	1999	23	5.1	121	1.33	0.13	0.688	5.96	0.261	0.304	0.0343	1629
DC93	1967	16	1.0	130	2.13	0.27	0.556	4.64	0.211	0.257	0.0343	1244
RJ1H	1987	13	5.1	124	1.43	0.18	0.688	5.68	0.218	0.274	0.0427	1529

Table 2. *Principal characteristics of a range of turbofan powered civil transport aircraft; the design optimum conditions are those at which* $(\eta_o L/D)$ *has its maximum value for an aircraft with a mass equal to 80% of the maximum permitted take-off value cruising in the ISA*

ICAO	S_{ref} (m²)	s (m)	b_f (m)	λ_ω (deg)	ψ_0	ψ_6	M_{DO}	$(R^{ac})_{DO}$	$(C_L)_{DO}$	$(M_{TF})^{ac}$	J_1	J_2	$(FL)_{MO}$	M_{MO}
A30B	260.0	44.83	5.64	28.0	8.77	0.693	0.753	9.25E+07	0.548	0.712	0.074	0.868	390	0.82
A306	260.0	44.84	5.64	28.0	7.80	0.716	0.753	9.86E+07	0.519	0.721	0.076	0.871	410	0.82
A310	219.0	43.89	5.64	28.0	8.38	0.657	0.772	8.14E+07	0.558	0.744	0.073	0.869	410	0.84
A313	219.0	43.89	5.64	28.0	8.21	0.711	0.772	8.69E+07	0.564	0.738	0.075	0.870	410	0.84
A318	122.4	34.10	3.95	25.0	7.47	0.607	0.753	5.42E+07	0.564	0.754	0.075	0.871	410	0.82
A319	122.4	34.10	3.95	25.0	7.70	0.656	0.753	5.81E+07	0.569	0.755	0.075	0.871	410	0.82
A320	122.4	34.10	3.95	25.0	8.40	0.656	0.753	5.59E+07	0.590	0.750	0.073	0.869	410	0.82
A321	122.4	34.15	3.95	25.0	8.63	0.794	0.753	6.51E+07	0.606	0.740	0.074	0.869	391	0.82
A332	361.6	60.30	5.64	29.7	6.69	0.645	0.786	1.10E+08	0.528	0.762	0.076	0.872	410	0.86
A333	361.6	60.30	5.64	29.7	6.90	0.645	0.786	1.09E+08	0.535	0.761	0.076	0.872	410	0.86
A338	374.0	64.00	5.64	30.0	6.21	0.648	0.786	1.12E+08	0.530	0.781	0.078	0.874	415	0.86
A339	374.0	64.00	5.64	30.0	6.46	0.648	0.786	1.10E+08	0.539	0.779	0.077	0.873	415	0.86
A342	361.6	60.30	5.64	29.7	7.08	0.711	0.786	1.16E+08	0.551	0.760	0.077	0.872	415	0.86
A343	361.6	60.30	5.64	29.7	7.38	0.711	0.786	1.14E+08	0.561	0.757	0.076	0.872	415	0.86
A345	437.3	63.45	5.64	31.1	6.73	0.831	0.796	1.53E+08	0.512	0.762	0.078	0.874	415	0.86
A346	437.3	63.45	5.64	31.1	7.06	0.822	0.796	1.49E+08	0.523	0.759	0.077	0.873	415	0.86
A359	445.0	64.75	5.96	32.0	6.14	0.569	0.820	1.21E+08	0.493	0.791	0.078	0.874	431	0.89
A35K	465.0	64.75	5.96	32.0	6.18	0.625	0.820	1.34E+08	0.500	0.789	0.078	0.874	415	0.89
A388	845.0	79.80	7.14	30.0	6.13	0.620	0.820	1.95E+08	0.446	0.794	0.082	0.876	431	0.89
BCS1	115.0	32.50	3.51	26.0	7.34	0.576	0.754	4.88E+07	0.576	0.776	0.076	0.873	410	0.82
BCS3	115.0	32.50	3.51	26.0	7.72	0.641	0.754	5.35E+07	0.585	0.775	0.075	0.872	410	0.82
A20N	122.4	35.10	3.59	25.0	7.52	0.705	0.753	5.94E+07	0.598	0.786	0.076	0.873	410	0.82
A21N	122.4	35.27	3.95	25.0	8.08	0.835	0.753	6.60E+07	0.626	0.777	0.077	0.873	391	0.82
B712	92.8	28.40	3.40	25.0	8.72	0.748	0.700	5.12E+07	0.594	0.685	0.073	0.867	371	0.82
B722	157.9	32.92	3.76	32.0	7.90	0.554	0.770	6.49E+07	0.499	0.687	0.072	0.865	420	0.90
B732	99.0	28.35	3.76	25.0	8.41	0.669	0.700	5.02E+07	0.556	0.678	0.073	0.867	370	0.82
B733	102.0	28.90	3.76	25.0	9.20	0.700	0.729	5.39E+07	0.578	0.715	0.072	0.867	390	0.82
B734	102.5	28.90	3.76	25.0	8.90	0.774	0.729	5.86E+07	0.579	0.710	0.074	0.868	370	0.82

Table 2. *Continued.*

ICAO	S_{ref} (m²)	s (m)	b_f (m)	λ_ω (deg)	ψ_0	ψ_6	M_{DO}	$(R^{ac})_{DO}$	$(C_L)_{DO}$	$(M_{TF})^{ac}$	J_1	J_2	$(FL)_{MO}$	M_{MO}
B735	103.7	28.90	3.76	25.0	8.33	0.681	0.729	5.55E+07	0.550	0.721	0.074	0.870	370	0.82
B736	124.6	34.30	3.76	25.0	7.42	0.567	0.758	5.14E+07	0.564	0.759	0.075	0.871	410	0.82
B737	124.6	34.30	3.76	25.0	7.61	0.607	0.758	5.46E+07	0.567	0.758	0.075	0.871	410	0.82
B738	124.6	34.30	3.76	25.0	8.18	0.684	0.758	6.01E+07	0.581	0.754	0.074	0.870	410	0.82
B739	124.6	34.32	3.76	25.0	7.93	0.737	0.758	6.42E+07	0.585	0.749	0.075	0.871	410	0.82
B37M	121.9	33.26	3.76	25.0	7.59	0.700	0.763	6.22E+07	0.573	0.779	0.076	0.872	410	0.82
B38M	121.9	33.26	3.76	25.0	7.87	0.720	0.763	6.31E+07	0.581	0.777	0.075	0.872	410	0.82
B39M	121.9	33.26	3.76	25.0	8.06	0.770	0.763	6.50E+07	0.599	0.769	0.076	0.872	410	0.82
B742	511.0	59.64	6.50	37.5	7.02	0.687	0.810	1.58E+08	0.458	0.692	0.074	0.868	450	0.90
B743	511.0	59.64	6.50	38.5	6.88	0.698	0.810	1.62E+08	0.453	0.683	0.073	0.867	450	0.90
B744	547.0	64.44	6.50	37.5	6.69	0.685	0.810	1.62E+08	0.465	0.698	0.074	0.869	450	0.92
B748	594.0	68.40	6.50	37.5	6.25	0.669	0.830	1.72E+08	0.458	0.732	0.077	0.872	421	0.90
B752	189.0	38.06	3.76	25.0	7.10	0.623	0.772	8.01E+07	0.497	0.770	0.078	0.874	420	0.86
B753	189.0	38.06	3.76	25.0	7.59	0.673	0.772	8.20E+07	0.522	0.760	0.078	0.873	430	0.86
B762	283.3	47.57	5.03	31.5	6.96	0.657	0.772	1.02E+08	0.500	0.719	0.076	0.871	430	0.86
B763	283.3	47.57	5.03	31.5	6.30	0.582	0.772	9.73E+07	0.470	0.730	0.077	0.873	431	0.86
B764	283.3	51.92	5.03	31.5	7.20	0.748	0.772	1.05E+08	0.544	0.723	0.075	0.870	450	0.86
B77L	427.8	64.80	6.20	31.6	6.50	0.765	0.811	1.43E+08	0.519	0.772	0.078	0.873	431	0.89
B772	427.8	60.93	6.20	31.6	6.46	0.632	0.811	1.29E+08	0.495	0.767	0.078	0.874	431	0.89
B77W	427.8	64.80	6.20	31.6	7.16	0.774	0.811	1.40E+08	0.542	0.767	0.076	0.872	431	0.89
B773	427.8	60.93	6.20	31.6	7.07	0.659	0.811	1.29E+08	0.515	0.760	0.077	0.872	431	0.89
B788	377.0	60.12	5.77	32.2	6.38	0.563	0.815	1.06E+08	0.508	0.784	0.077	0.873	431	0.90
B789	377.0	60.12	5.77	32.2	6.48	0.627	0.815	1.16E+08	0.509	0.784	0.077	0.873	431	0.90
B78X	377.0	60.12	5.77	32.2	6.61	0.627	0.815	1.17E+08	0.513	0.782	0.077	0.873	411	0.90
E75S	83.0	25.00	3.00	22.5	7.85	0.560	0.733	4.09E+07	0.552	0.742	0.075	0.871	410	0.82
E75L	83.0	25.00	3.00	22.5	7.97	0.560	0.733	4.06E+07	0.556	0.741	0.075	0.871	410	0.82
E135	51.2	20.04	2.25	22.5	8.02	0.487	0.704	2.64E+07	0.562	0.709	0.074	0.869	370	0.78
E145	51.2	20.04	2.25	22.5	8.38	0.536	0.704	2.87E+07	0.570	0.706	0.073	0.868	370	0.78
E170	72.7	25.30	3.15	22.5	8.10	0.589	0.733	3.72E+07	0.598	0.744	0.074	0.869	410	0.82

Table 2.   Continued.

ICAO	S_{ref} (m^2)	s (m)	b_f (m)	λ_ω (deg)	ψ_0	ψ_6	M_{DO}	$(R^{ac})_{DO}$	$(C_L)_{DO}$	$(M_{TF})^{ac}$	J_1	J_2	$(FL)_{MO}$	M_{MO}
E190	86.0	27.71	2.74	22.5	7.90	0.599	0.758	4.28E+07	0.594	0.770	0.074	0.870	410	0.82
E195	92.5	27.73	3.00	22.5	8.13	0.569	0.758	4.29E+07	0.584	0.766	0.074	0.870	410	0.82
E290	110.0	33.72	3.00	22.5	6.99	0.552	0.758	4.59E+07	0.578	0.806	0.078	0.874	410	0.82
E295	110.0	35.12	3.00	22.5	7.52	0.602	0.758	4.72E+07	0.613	0.805	0.076	0.873	410	0.82
MD82	112.3	32.85	3.35	22.5	8.96	0.721	0.720	5.43E+07	0.612	0.715	0.072	0.866	370	0.84
MD83	112.3	32.85	3.35	22.5	8.86	0.772	0.720	5.77E+07	0.622	0.709	0.073	0.867	370	0.84
GLF5	105.6	28.50	2.50	25.0	6.70	0.406	0.772	3.83E+07	0.508	0.765	0.077	0.873	510	0.89
CRJ9	69.0	22.62	2.69	26.0	7.94	0.607	0.753	4.17E+07	0.550	0.737	0.074	0.869	410	0.85
DC93	93.0	28.44	3.35	24.0	7.95	0.606	0.733	4.58E+07	0.565	0.719	0.074	0.868	370	0.84
RJ1H	77.3	26.34	3.50	15.0	9.77	0.838	0.650	4.49E+07	0.637	0.682	0.074	0.869	350	0.73

where s is the wingspan, e_{LS} is the low-speed Oswald efficiency factor and Cd_0 is the zero-lift drag coefficient. As described in Poll and Schumann [4], Cd_0 is related to the mean skin friction coefficient, C_F, by

$$Cd_0 = \psi_0 C_F^{ac}, \tag{32}$$

where ψ_0 depends upon the aircraft geometry and, as shown in Poll and Schumann [3], the variation of C_F with Reynolds number at Mach 0.5 can be approximated by a simple power law with constant coefficients, i.e.

$$C_F^{ac} \approx \frac{a}{(R^{ac})^b} = \frac{0.0269}{(R^{ac})^{0.14}}. \tag{33}$$

Here, the aircraft flight Reynolds number, R^{ac}, is defined as

$$R^{ac} = \frac{l \rho_\infty V_\infty}{\mu_\infty} = S_{ref}^{1/2} \left(\frac{\rho_\infty a_\infty}{\mu_\infty} \right) M_\infty = S_{ref}^{1/2} \left(\frac{\gamma p_\infty}{\mu_\infty a_\infty} \right) M_\infty, \tag{34}$$

where, l is a typical aircraft reference length, taken to be the square root of the reference wing area, a_∞ the local speed of sound and μ_∞ the dynamic viscosity.

As described in Refs (3) and (4), the Oswald factor is a function of Cd_0 and aircraft geometry such that, from Equations (26), (27) and (28) of Ref. (4),

$$e_{LS} \approx \frac{1}{1.03 + \delta_2 + \pi.AR.k_1}, \tag{35}$$

where

$$\delta_2 \approx 2 \left(\frac{b_f}{s} \right)^2 \tag{36}$$

and

$$k_1 \approx 0.80 \, (1 - 0.53 \cos(\Lambda_w)) \, Cd_0, \tag{37}$$

with b_f being the fuselage maximum width and Λ_w the wing quarter-chord sweep angle. Therefore,

$$K = \frac{1}{\pi.AR.e_{LS}} \approx k_1 + \left(\frac{1.03 + \delta_2}{\pi.AR} \right). \tag{38}$$

The zero-lift drag coefficient, Cd_0, is the sum of the pressure, or form, drag and the surface skin friction drag. At low Mach numbers, the form drag increases with increasing Mach number, whilst the skin friction drag decreases. Above a Mach number of about 0.5 these effects are approximately equal. Consequently, Cd_0 and, hence, K may be assumed to be independent of Mach number.

At higher Mach numbers, the drag polar is modified by the effects of compressibility and the general form becomes

$$Cd = function \, (C_L, M_\infty, R^{ac}) \approx Cd_0 + KC_L^2 + Cd_w, \tag{39}$$

where Cd_w is the wave drag coefficient. If Cd_0 and K are independent of Mach number, Cd_w must capture all the compressibility effects, up to and including the development of regions of supersonic flow and, ultimately, the formation of shockwaves. When defined in this way, the wave drag coefficient is a function of Mach number, lift coefficient and, to a lesser extent, Reynolds number – see Shevell [11].

As the flight speed increases, sonic conditions are eventually reached at the point on the wing where the local static pressure is lowest. Further increases lead to the formation of a region of supersonic flow bounded by the wing surface, a sonic interface[9] in the region adjacent to the surface and a terminating shockwave. Once this local supersonic zone is established, the terminating shockwave moves rearwards and strengthens when either the Mach number, or the lift coefficient is increased. Whilst this zone is confined to the front portion of the wing, the associated drag increase is small, being typically less

---

[9]The surface formed by all the points in the flow field where the local Mach number is unity.

than about 10 drag counts[10] and this variation is known as drag creep. However, when the terminating shockwave moves onto the rear part of the wing, it strengthens. Consequently, the drag changes following increases in M_∞, or C_L, become much larger and this more rapid variation is referred to as drag rise.

According to the Poll and Schumann [5] model, which is based upon ideas by Shevell [11], transition from drag creep to drag rise is governed by the local Mach number at the wing crest. This is the point on the aerofoil where the surface slope is parallel to the undisturbed freestream direction. The drag rise begins when supersonic flow is established downstream of the crest and this occurs when the freestream Mach number exceeds a threshold value known as the crest critical Mach number, M_{cc}. This quantity depends, primarily, upon wing geometry and the lift coefficient, whilst the magnitude of the wave drag is governed by the ratio of M_∞ to M_{cc}. Hence, the variable controlling the wave drag is taken to be

$$X = \frac{M_\infty \cos(\Lambda_w)}{(M_{CC})^{ac}}, \tag{40}$$

where

$$(M_{CC})^{ac} = (M_{TF})^{ac} - 0.10 \left(\frac{C_L}{\cos^2(\Lambda_w)} \right). \tag{41}$$

Here, $(M_{TF})^{ac}$ is a constant aircraft characteristic that captures the aerofoil technology level and the distribution of wing thickness-to-streamwise chord ratio across the span.

In the drag creep region,

$$(Cd_w)_{creep} \approx \cos^3(\Lambda_w) \left(j_1(X - j_2)^2 \right), \tag{42}$$

where j_1 and j_2 are constant aircraft dependent characteristics. If X is less than j_2, the wave drag is zero and the drag creep region is deemed to have ended when X reaches the design optimum value, X_{DO}, where, from Equations (40) and (41),

$$X_{DO} = \frac{M_{DO} \cos(\Lambda_w)}{(M_{TF})^{ac} - 0.10 \left(\frac{(C_L)_{DO}}{\cos^2(\Lambda_w)} \right)}. \tag{43}$$

At larger values of X, i.e. in the drag rise region, an additional term is introduced to capture the effect of strengthening shock waves. Hence,

$$(Cd_w)_{rise} \approx \cos^3(\Lambda_w) \left(j_1(X - j_2)^2 + j_3(X - X_{DO})^4 \right), \tag{44}$$

where j_3 is also a constant and is currently taken to be 40. Values of j_1 and j_2 are given in Table 2.

At all flight conditions, the lift-to-drag ratio is given by

$$\frac{L}{D} = \frac{C_L}{Cd} = \frac{C_L}{\left(Cd_0 + KC_L^2 + Cd_w \right)}. \tag{45}$$

By way of illustration, the variation of *L/D* with drag coefficient and Mach number at a fixed total mass for the A320 has been estimated using the Equations (30)–(45) with the input parameters given in Table 2. The results are presented in Fig. 3. As expected, the maximum value of *L/D* and the corresponding drag coefficient decrease as the flight Mach number increases.

5.0 The operational limits

Whilst the model is valid over a wide range of conditions, there are four principal performance factors that can limit the achievable combinations of Mach number and flight level in normal operations.

---

[10] 1 drag count is equal to a change of 0.0001 in Cd.
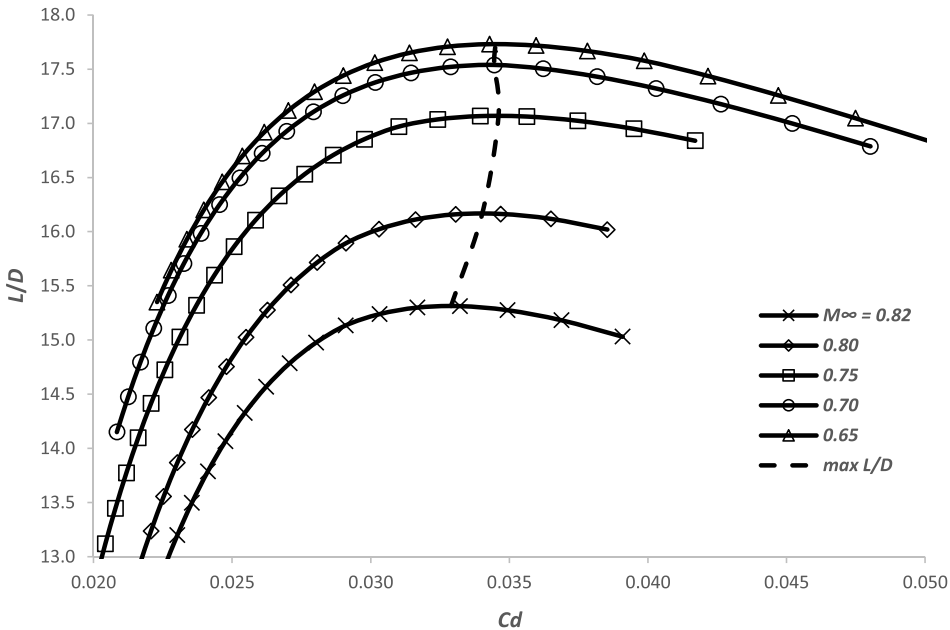
Figure 3. *Approximate variation of lift-to-drag ratio for the A320 aircraft with drag coefficient and Mach number operating at a total mass of 58,800kg.*

5.1. Maximum lift limit

The first constraint is the lift limit, sometimes referred to as the 'manoeuvre' limit, which is linked to the conditions at which wing buffeting[11] is first encountered during a specified manoeuvre – usually a level turn. For a given aircraft weight, the onset of buffeting defines an envelope of maximum achievable flight level for straight and level flight as a function of Mach number. This envelope also has a local maximum, i.e. at a given weight, there is an absolute maximum flight level and this is referred to as the "aerodynamic" ceiling.

Starting immediately after take-off, the aircraft must stay above the minimum speed dictated by maximum usable wing lift. In straight and level flight at low speed, the wing stalls at a particular value of the lift coefficient, $(C_L)_{stall}$, known as the 1g stall condition. However, the stall is preceded by buffeting beginning at $(C_L)_{buff}$, which is about 90% of $(C_L)_{stall}$. In addition, to give the aircraft some margin for safe manoeuvre in an emergency, it is a regulatory requirement that the maximum useable lift coefficient, $(C_L)_{mu}$, in straight and level flight be set at a value that allows a 1.3g manoeuvre, e.g. a 40° level banked turn, to be executed before buffet onset, i.e.

$$(C_L)_{MU} = \frac{(C_L)_{buff}}{1.3} \approx \frac{(C_L)_{stall}}{1.5}, \tag{46}$$

Data given in Obert [13] suggests that, for aircraft in the clean configuration at low Mach number, $(C_L)_{stall}$ is about 1.4 ±0.3, whilst, from Table 2, the average value of $(C_L)_{DO}$ is seen to be about 0.55. Hence, at low speed, the ratio of $(C_L)_{mu}$ to $(C_L)_{DO}$ is about 1.8 ±0.4. Clean condition values are applicable for flight above 3,000 feet (*FL*>30), since at lower altitudes high-lift devices are likely to be used and, consequently, $(C_L)_{mu}$ will be much higher.

At high speeds, as Mach number increases, the shock waves on the wing eventually become strong enough to cause local, boundary-layer separation and the shock wave system itself may become unsteady.

---

[11]As an aerodynamic limit is approached, the first signs are usually weak, unsteady pressure variations in the flow. These are sensed by the pilot as vibrations of the aircraft structure, which are described, qualitatively, as "buffeting".
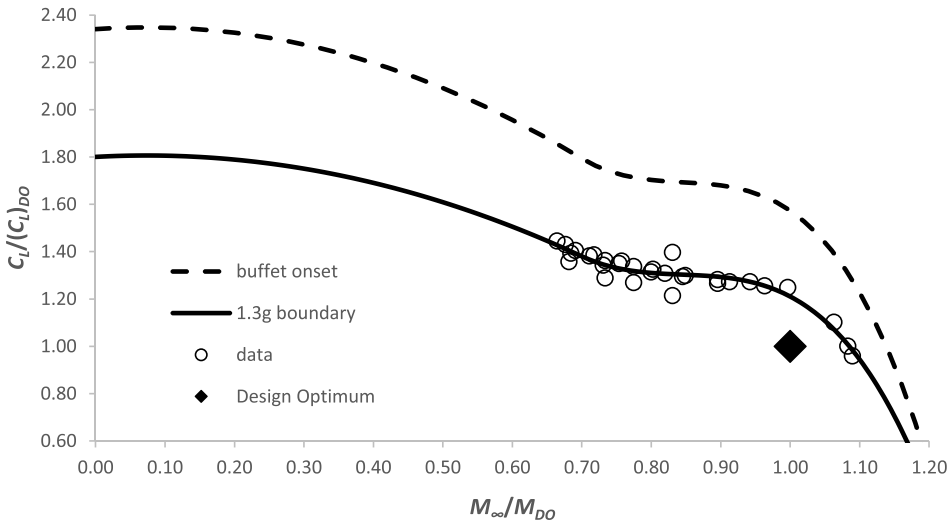
Figure 4. *An estimate of the normalised 1g buffet onset and 1.3g manoeuvre boundaries for a typical civil transport aircraft in the clean condition. Data are taken from an FCOM and the centre of gravity is 35% of the mean aerodynamic chord.*

This also produces time varying forces that present as buffeting. Further increases in speed produce major changes in the wing flow, eventually leading to a situation in which the aircraft can no longer be controlled. This phenomenon is known as the high-speed stall and, for safety reasons, at each Mach number, a maximum usable, lift coefficient is imposed such that, relative to straight and level flight, and consistent with the low-speed stall, the aircraft must be able to execute a 1.3g level turn without encountering any buffeting.

Typical 1g buffet onset and 1.3g manoeuvre boundaries are shown in Fig. 4. Here, the solid line is a smoothed, empirical estimate of the typical manoeuvre boundary linking the low-speed limit of $(C_L)_{mu}/(C_L)_{DO}$ equal to approximately 1.8 and the high-speed limit based upon data taken from the charts given in the Flight Crew Operating Manual (*FCOM*) of a typical civil transport aircraft. In general, the boundary depends upon the location of the aircraft's centre of gravity and an average value of 35% of the mean aerodynamic chord has been assumed. More information can be found in Obert [13] Chapter 26 for the low-speed stall and Chapter 28 for buffet onset at high speed. The data are normalised using $(C_L)_{DO}$ and M_{DO} and, in this form, the curves are expected to be broadly similar for all the aircraft considered here. The solid diamond symbol shows the flight condition for $(\eta_o L/D)_{DO}$ and the manoeuvre boundary loops around it, leaving a clear margin of safety before the stall.

Using the definition of lift coefficient given in Equation (16), the variation of $(p_\infty)_{min}$ with Mach number at the manoeuvre boundary is given by

$$\frac{(p_\infty)_{DO}}{(p_\infty)_{min}} = 0.8 \left(\frac{(C_L)_{MU}}{(C_L)_{DO}} \right) \left(\frac{MTOM}{m} \right) \left(\frac{M_\infty}{M_{DO}} \right)^2, \tag{47}$$

whilst the static pressure at the design optimum condition is,

$$\frac{(p_\infty)_{DO}}{(p_{TP})_{ISA}} = \frac{0.80}{(C_L)_{DO}} \psi_6, \tag{48}$$

where $(p_{TP})_{ISA}$ is the static pressure at the tropopause in the International Standard Atmosphere [9] and, using the notation from Poll and Schumann [4],

$$\psi_6 = \left(\frac{MTOM.g}{(\gamma/2)(p_{TP})_{ISA} M_{DO}^2 S_{ref}} \right). \tag{49}$$

Values of ψ_6 are given in Poll and Schumann [5] and are also listed in Table 2.
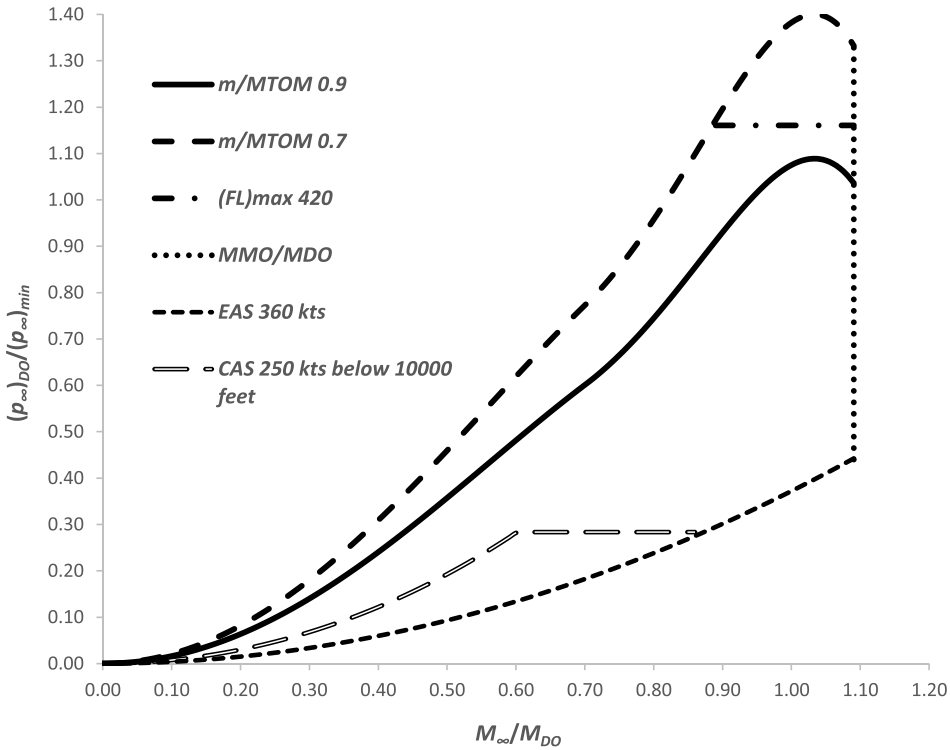
Figure 5. *Variation of the minimum static pressure (maximum flight level) with Mach number for the approximate manoeuvre boundary for two values of aircraft mass. Also shown is a typical cabin pressure limit (FL 420), together with a typical maximum operational Mach number limit and an approximate structural strength boundary ($(V_{EAS})_{MO}$ of 360 kt), plus an alternative ATM limit of 250 kt CAS below 10,000 feet.*

Static pressure is linked directly to the flight level through Equations (A13) and (A14) in Appendix B, i.e., if $(p_{\infty}/(p_{SL})_{ISA})$ is greater than 0.223363,

$$FL = 1454.4302 \left(1 - \left(\frac{p_{\infty}}{(p_{SL})_{ISA}} \right)^{0.190263} \right), \tag{50}$$

otherwise

$$FL = 49.02022 \left(1 - 4.24436 ln \left(\frac{p_{\infty}}{(p_{SL})_{ISA}} \right) \right). \tag{51}$$

Relations for the approximate variation of normalised $(C_L)_{mu}$ with normalised Mach number are given in Appendix D and the form of the manoeuvre boundary, expressed as a normalised pressure versus normalised Mach number, is given in Fig. 5. As the aircraft climbs, the Mach number for the onset of the low-speed stall increases, whilst that for high-speed stall decreases. Eventually, a condition is reached at which both begin at the same Mach number. The resulting flight level is an absolute maximum and this is the aircraft's aerodynamic ceiling. From Equation (D4), it is found that the Mach number at this condition, $(M_{\infty})_{AC}$, is given by

$$(M_{\infty})_{AC} \approx 1.035 M_{DO} \tag{52}$$

and $(p_\infty)_{AC}$ is

$$\frac{(p_\infty)_{DO}}{(p_\infty)_{AC}} \approx 0.544 \left(\frac{(C_L)_{mu}}{(C_L)_{DO}} \right)_{LS} \left(\frac{MTOM}{m} \right) \approx 0.98 \left(\frac{MTOM}{m} \right). \tag{53}$$

Clearly, the aerodynamic ceiling is strongly dependent upon the aircraft mass.

5.2. Maximum thrust limit

The next constraint is the thrust limit, sometimes referred to as the minimum available climb rate. This is governed by the engine's net thrust when it is operating at its maximum continuous climb rating. The engine rating is usually determined by specifying a maximum value for the total temperature of the mixture of air and the products of combustion at the entry to the engine's turbine section, i.e. the turbine entry temperature, or *TET*. As described in Ref. (6), the maximum continuous climb value, $(TET)_{MCC}$, is about 0.92 times the maximum at take-off value, $(TET)_{MTO}$. With the engine at maximum continuous climb, the achievable rate of climb at a given Mach number decreases as the altitude increases and the maximum useful operational altitude is deemed to have been reached when it drops to about 300 feet/minute. This is called the service ceiling for that Mach number.

From Equations (8) and (9), assuming small angles and neglecting small terms, when the airspeed is constant, the residual available rate of climb is

$$\frac{dh}{dt} \approx V_\infty \frac{(n.F_n - D)}{mg_n} = M_\infty a_\infty \frac{(C_T - Cd)}{C_L}, \tag{54}$$

With the engines at maximum continuous climb, the thrust coefficient is $(C_T)_{MCC}$ and when the rate of climb is 300 feet/min, the corresponding service-ceiling, lift coefficient, $(C_L)_{SC}$, is obtained using Equations (39) and (54),

$$K (C_L)_{SC}^2 + \frac{0.00516}{M_\infty} \left(\frac{(T_{TP})_{ISA}}{T_\infty} \right)^{1/2} (C_L)_{SC} - ((C_T)_{MCC} - (Cd_0 + Cd_w)) = 0, \tag{55}$$

where $(T_{TP})_{ISA}$ is the temperature at the tropopause in the International Standard Atmosphere. An exact solution of this equation requires several iterations.

Sample calculations have been performed for values of *m/MTOM* equal to 0.9 and 0.7, with ambient temperatures of *ISA* and *ISA* +20°C. The results are given Figs 6 and 7. As expected, the thrust limited boundaries exhibit maxima corresponding to the highest achievable service ceilings. Changing weight has a major effect and increasing the ambient temperature reduces the service ceiling significantly.

Whilst the full calculation is complex, the exact solutions show that the static pressure at the service ceiling is not particularly sensitive to the Mach number. Consequently, a reasonable approximate solution is given by determining $(C_L)_{SC}$ at the design optimum Mach number, M_{DO}. As shown in Appendix E, this has the form

$$\frac{(C_L)_{SC}}{(C_L)_{DO}} \approx \left(c_1 \left(\frac{(TET)_{MCC}}{T_\infty} \right) + c_2 \right)^{1/2} - c_3 \left(\frac{(T_{TP})_{ISA}}{T_\infty} \right)^{1/2}, \tag{56}$$

where the coefficients c_1, c_2 and c_3 are constant and functions of the aircraft parameters at the design optimum condition, as shown in Equations (E11), (E12) and (E13). The resulting values of static pressure ratio are obtained from Equation (47), i.e.

$$\frac{(p_\infty)_{DO}}{(p_\infty)_{SC}} \approx 0.8 \left(\frac{(C_L)_{SC}}{(C_L)_{DO}} \right) \left(\frac{MTOM}{m} \right). \tag{57}$$

The service ceiling static pressure is proportional to the aircraft mass and, since, as indicated in Equation (56), $(C_L)_{SC}$ decreases as atmospheric temperature increases, it also increases as the atmospheric temperature increases. Hence, the service ceiling flight level decreases as both mass and atmospheric temperature increase.
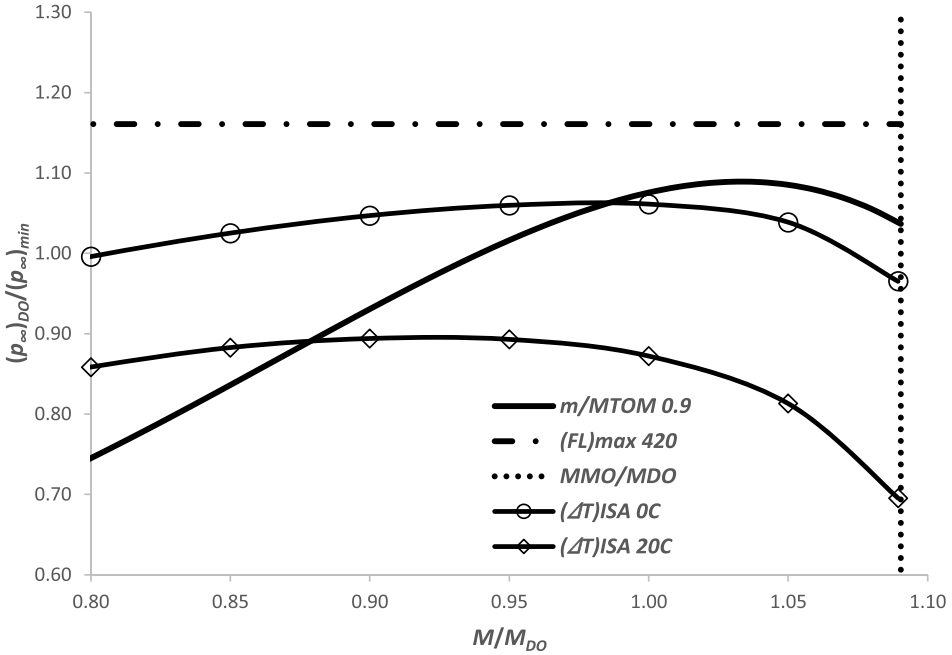
Figure 6. *Variation of the minimum static pressure with Mach number for the thrust limited boundary when m/MTOM is equal to 0.9 and for ISA ambient temperature and ISA+20°C. Also shown is manoeuvre limit for m/MTOM equal to 0.9, plus the cabin pressure limit (FL 420), together with a typical maximum operational Mach number.*
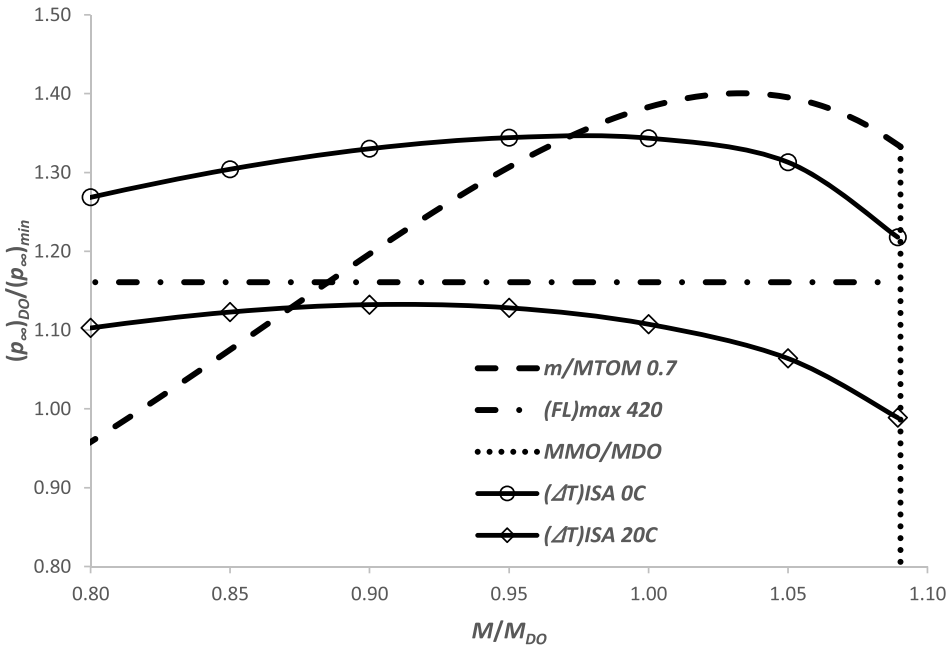
Figure 7. *The same Fig. 6, but for m/MTOM is equal to 0.7.*

5.3. Maximum permitted flight level

The third restriction is the maximum cabin pressure limit. This is a structural strength constraint that fixes the maximum allowable difference between the internal cabin pressure and the external atmospheric pressure. It takes the form of a maximum permitted flight level, FL_{max}, given in the Type Certificate Data Sheet (*TCDS*), and, for civil transport aircraft, it is, typically, about *FL* 410. Once again, this can be expressed as a ratio of static pressures, i.e. using Equations (47), (48) and (53),

$$\frac{(p_\infty)_{DO}}{(p_\infty)_{min}} = 0.8 \frac{\psi_6}{(C_L)_{DO}} \left(\frac{(p_{TP})_{ISA}}{(p_\infty)_{min}} \right) = 0.1412 \frac{\psi_6}{(C_L)_{DO}} EXP \left(\frac{FL_{max}}{208.06} \right). \tag{58}$$

Results for this limit are included in Figs 5, 6 and 7.

In these examples, when the ambient temperature has the *ISA* value, the service ceiling and the aerodynamic ceiling are close together. At the higher aircraft weight, as shown in Fig. 6, both ceilings are below the cabin pressure limit and so the service ceiling is the greatest height that the aircraft can reach. Conversely, at the lower aircraft weight given in Fig. 7, both the service and the aerodynamic ceilings lie above the cabin pressure limit and so the maximum achievable flight level is determined by the cabin pressure limit. However, when the ambient temperature is increased to *ISA* $+20°C$, the service ceiling determines the maximum achievable altitude at both weights.

5.4. Maximum speed limit

Finally, the fourth constraint is the maximum operational speed. This is also a structural strength constraint. At low altitudes, this is usually expressed as a maximum permitted value of the dynamic pressure, $(q_\infty)_{MO}$, which, as shown in Appendix B, is equivalent to a maximum value of the equivalent airspeed, $(V_{EAS})_{MO}$, i.e.

$$(q_\infty)_{MO} = \frac{\gamma}{2} (p_{SL})_{ISA} \left(\frac{(V_{EAS})_{MO}}{(a_{SL})_{ISA}} \right)^2 = \frac{\gamma}{2} p_\infty M_\infty^2. \tag{59}$$

Therefore, at a given Mach number, there is a maximum permitted freestream static pressure, corresponding to a minimum permitted flight level, where

$$(p_\infty)_{max} = \frac{2(q_\infty)_{MO}}{\gamma M_\infty^2} = (p_{SL})_{ISA} \left(\frac{(V_{EAS})_{MO}}{M_\infty (a_{SL})_{ISA}} \right)^2, \tag{60}$$

or, using Equation (48),

$$\frac{(p_\infty)_{DO}}{(p_\infty)_{max}} \approx 0.8 \left(\frac{\psi_6 M_{DO}^2}{(C_L)_{DO}} \right) \left(\frac{p_{TP}}{p_{SL}} \right)_{ISA} \left(\frac{(a_{SL})_{ISA}}{(V_{EAS})_{MO}} \right)^2 \left(\frac{M_\infty}{M_{DO}} \right)^2. \tag{61}$$

At high altitude, $(V_{EAS})_{MO}$ is replaced by a maximum operational Mach number, M_{MO}. Constant equivalent airspeed gives way to constant Mach number at the crossover flight level, $(FL)_{CO}$, which is obtained from Equation (61), i.e.

$$\frac{(p_\infty)_{DO}}{(p_\infty)_{CO}} \approx 0.8 \frac{\psi_6}{(C_L)_{DO}} \left(\frac{p_{TP}}{p_{SL}} \right)_{ISA} \left(\frac{M_{MO}(a_{SL})_{ISA}}{(V_{EAS})_{MO}} \right)^2. \tag{62}$$

Values of $(V_{EAS})_{MO}$ and M_{MO} usually appear in the aircraft's *TCDS* and, whilst there is a relationship between the two, it is complex and beyond the scope of a simple representation. Nevertheless, data presented by Jenkinson et al. [14] suggest that there is a rough correlation, with an uncertainty of about ± 10%,

$$\frac{(V_{EAS})_{MO}}{(a_{SL})_{ISA}} \approx 0.57 \left(M_{MO} + 0.10 \right). \tag{63}$$

Therefore, approximate values of $(V_{EAS})_{MO}$ can been obtained from Equation (63) using the values of M_{MO} given in Table 2.

Finally, below 10,000 feet, there may be a limit on the calibrated airspeed, $(V_{CAS})_{MO}$, imposed by air traffic control. Typically, this would be 250 kt. The relation between calibrated airspeed and Mach number is obtained by combining Equations (B1) and (B5) from Appendix B, which together with Equation (48) gives the relationship between maximum static pressure (minimum flight level) and Mach number to be

$$\frac{(p_\infty)_{DO}}{(p_\infty)_{\max}} \approx 0.8 \frac{\psi_6}{(C_L)_{DO}} \left(\frac{p_{TP}}{p_{SL}}\right)_{ISA} \left(\frac{\left(1 + \frac{(\gamma-1)}{2}M_{DO}^2\left(\frac{M_\infty}{M_{DO}}\right)^2\right)^{\frac{\gamma}{(\gamma-1)}} - 1}{\left(1 + \frac{(\gamma-1)}{2}\left(\frac{(V_{CAS})_{MO}}{(a_{SL})_{ISA}}\right)^2\right)^{\frac{\gamma}{(\gamma-1)}} - 1} \right). \tag{64}$$

A sample maximum operational speed boundary is included in Fig. 5 and it is independent of both the aircraft weight and the ambient temperature.

6.0 Determination of the fuel flow rate and engine overall efficiency in climb and cruise

For an aircraft of given total weight, the method's principal output parameters are the total fuel mass-flow rate and the engine overall efficiency. These quantities are obtained by applying the following computational scheme.

The input parameters are aircraft type, mass, Mach number, flight level, rate of climb, time rate of change of true airspeed and ambient temperature. With p_∞ determined from the definition of flight level and T_∞ specified, sound speed, a_∞, true airspeed, V_∞, and dynamic viscosity, μ_∞, follow. Lift coefficient and Reynolds number are then given by Equations (16) and (34). Values of AR, δ_2, C_F, Cd_0 and k_1 are obtained from Equations (31) to (37), followed by e_{LS} and K from Equations (35) and (38). The value of the crest critical Mach number, $(M_{CC})^{ac}$ is found from Equation (41) and X from Equation (40), whilst the wave drag coefficient comes from Equation (44). Values of the geometric parameters S_{ref}, s, b_f, and Λ_w, are listed in Table 2 together with the derived coefficients $\psi 0$, $(M_{TF})^{ac}$, $(C_L)_{DO}$, j_1 and j_2. Having obtained Cd_w, the estimate for L/D is obtained from Equation (45).

The estimation of η_o begins with the calculation of the total, net engine thrust using Equations (4) and (13), with the thrust coefficient, C_T, following from Equation (17). Using M_∞, M_{DO}, $(\eta_o)_{DO}$, $(C_T)_{DO}$ and η_2 from Equations (29), (27) and (28) give $(\eta_o)_B$ and $(C_T)_{\eta B}$. These quantities are then used in Equation (24) to give η_o. Values for the engine constants $(\eta_o)_{DO}$, $(C_T)_{DO}$ and BPR are given in Table 1 and M_{DO} is given in Table 2.

With the engine overall efficiency and the lift-to-drag ratio now determined, the fuel flow rate is given by Equation (19).
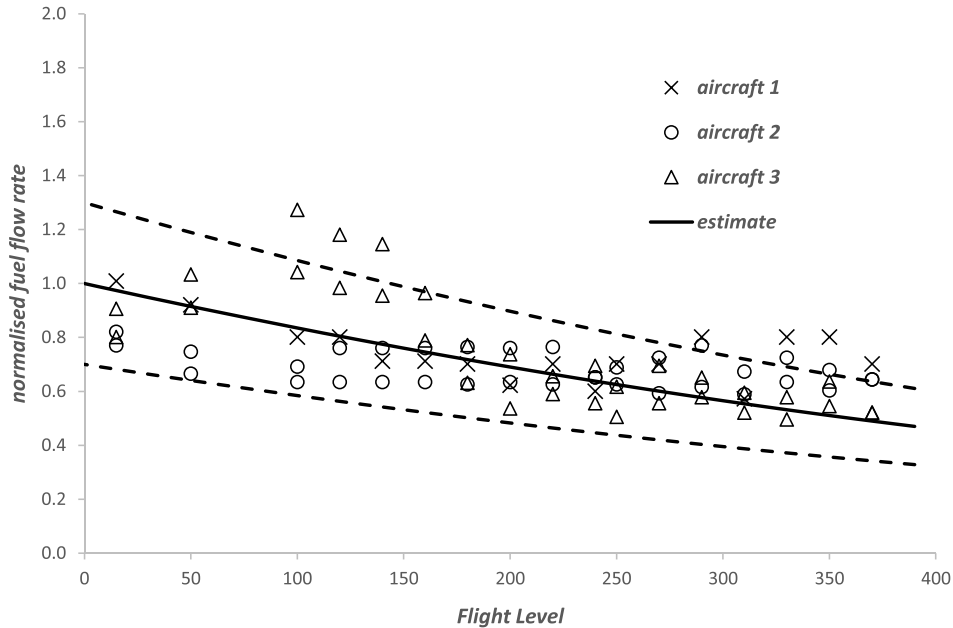
7.0 Fuel flow rate estimate for 'flight idle' operation in descent

During the descent phase, the throttles may be set to the flight idle position. In this mode, the net thrust is very low, possibly negative, and fuel is being used to keep the engine running at a safe minimum speed. Under these conditions, the compressor characteristics may be very different from those in climb and cruise and there may be variations in the various blade and engine bleed settings.

When developing the engine model, Poll and Schumann [6] made use of information given in Jenkinson et al. [14], which includes results for the descent phase. These indicate that, when the flight idle fuel flow rate is normalised with respect to its value at sea-level, static conditions, the result has a strong dependence upon altitude, but only a weak dependence upon Mach number and nominal bypass ratio. Since the engine is producing close to zero net thrust at this condition, unlike the other phases of flight, there is no dependence upon aircraft weight. Curve fitting the data gives

$$\left(\frac{\dot{m}_f}{(\dot{m}_f)_{SLS}}\right)_{FI} \approx 1 - 0.178\left(\frac{FL}{100}\right) + 0.0085\left(\frac{FL}{100}\right)^2. \tag{65}$$

Figure 8. *Variation of normalised, flight-idle, fuel flow rate with altitude for three aircraft. Open symbols are FCOM data. The solid line is the estimate from Equation (65) and the dashed lines show the ± 30% variation.*

Information on descent phase fuel flow is given in the aircraft's *FCOM* and, whilst these documents are not generally available in the public domain, some manuals and several extracts can be found on the internet. Fortunately, the *ICAO* Aircraft Engine Emissions Data Bank [15] lists fuel flow rates for the flight idle throttle setting at sea-level, static conditions for a large number of engines and these values are listed in Table 1. The combination of these data with Equation (65) yields an estimate of the flight idle fuel burn rate at any flight level.

Comparisons of *FCOM* data for three aircraft, one single aisle (aircraft 1) and two twin aisle (aircraft 2 and 3) are presented in Fig. 8, together with the estimates based upon Equation (64) and the *ICAO* data. The results exhibit a large degree of residual scatter, some of which is due to the difficulty of estimating instantaneous fuel flow rates from the *FCOM* tables. Nevertheless, the altitude dependence is clearly visible, as is the collapse achieved with the chosen normalising parameter.

Despite the complexity of the situation, this simplified expression produces estimates that are generally within 30% of the values derived from the limited *FCOM* data. This rather large uncertainty is offset by the fact that, as indicted by the data given in Table 1, the fuel burn rate at flight idle is an order of magnitude lower than that at take-off. Flight idle values should be used when the aircraft is descending and the estimated fuel flow rate drops below that given by Equation (65).

8.0 Fuel flow rate estimates for take-off, initial climb-out and approach and landing

Below 3,000 feet, the aircraft is likely to have its flaps fully, or partially, deployed and the undercarriage might be lowered. Clearly, this has a major effect on the drag and, since the method, in its current form, only addresses the clean configuration, for completeness, some means of estimating fuel flow rate in these other situations is required.

For all but the shortest flights, most of the fuel is consumed in the climb and cruise. Hence, high accuracy in other phases of flight is less important and, perhaps, the simplest approach is the use the

average landing and take-off (*LTO*) cycle specified for use with the *ICAO* Aircraft Engine Emissions Data Bank [15]. This gives the following recommendations.

1. At take-off, the aircraft operates at the maximum available thrust for 0.7 minutes.
2. During the initial climb out, the engine thrust is reduced to 85% of the maximum available for 2.2 minutes.

and

3. During the final approach for landing, the engine thrust is set to 30% of the maximum available thrust for 4.0 minutes.

If the engine type is known, the fuel flow rates can be read directly from the ICAO data base. However, in many situations, the engine model will not be known. Therefore, average values for maximum take-off thrust and corresponding fuel flow rates have been obtained for each aircraft type. This was done by taking the mean values for all the engine types fitted to each aircraft. These results are listed in Table 1.

In addition, it was found that, relative to maximum take-off values, when the thrust level is reduced to 85% and 30%, the fuel flow rate drops to 0.82±0.02% and 0.28±0.02%. Applying these factors gives the approximate fuel for climb-out and approach and landing.

The relative importance of the fuel used in these stages of flight depends upon how the aircraft is operated. For flights close to the maximum possible range, they represent about 5% of the total fuel used. However, for very short flights this can increase to over 25%.

9.0 Engine deterioration in service

The performance of both airframe and engines varies with time due to in-service deterioration – see, for example, Arrieta, Botez and Lasne [16]. In the case of the airframe, this is primarily the result of dirt accumulation on the outer surface and erosion, or damage, to the paint covering. There is also the possibility of rigging errors when major components, e.g. ailerons, are refitted following removal for inspection, or repair. All these can result in increased drag. However, this penalty is expected to be small. In the case of the engines, dirt is also a major issue, leading to a progressive reduction of component polytropic efficiencies through surface contamination (fouling) and surface erosion. There is also the progressive wearing of seals and bearings. These effects all lead to a steady increase in the rate at which fuel is burned for a given thrust.

As discussed in Ref. 16, engine degradation rate depends upon the operational cycle and the operating environment. Consequently, results for short haul and long haul are different. Airlines can take low-level remedial action, such as core washing, whilst the engine is still in service, or the engine can have a major overhaul. During its lifetime, an engine might undergo two, or three, complete overhauls and during its lifetime an aircraft may need two, or more, sets of new engines. This whole process is driven by airline economics. However, irrespective of the operational cycle, as indicated in Ref. 16, the maximum acceptable increase in fuel consumption before a maintenance intervention is likely to be in the region of 5%.

When the method is applied to a particular aircraft, it is unlikely that the degree of in-service deterioration will be known. However, as noted above, this extra fuel use is likely to be between 0 to 5%. Therefore, it is assumed that the method gives estimates that are representative of a nearly new aircraft and that the mean, in-service deterioration is taken to be 2.5%. To capture this, a multiplier of 0.975 is applied to the engine overall efficiency, i.e. the in-service overall efficiency is

$$(\eta_o)_{IS} \approx 0.975 \, (\eta_o) \, . \tag{66}$$

This corrected value is used in Equation (19) to obtain the final estimate of the fuel consumption.
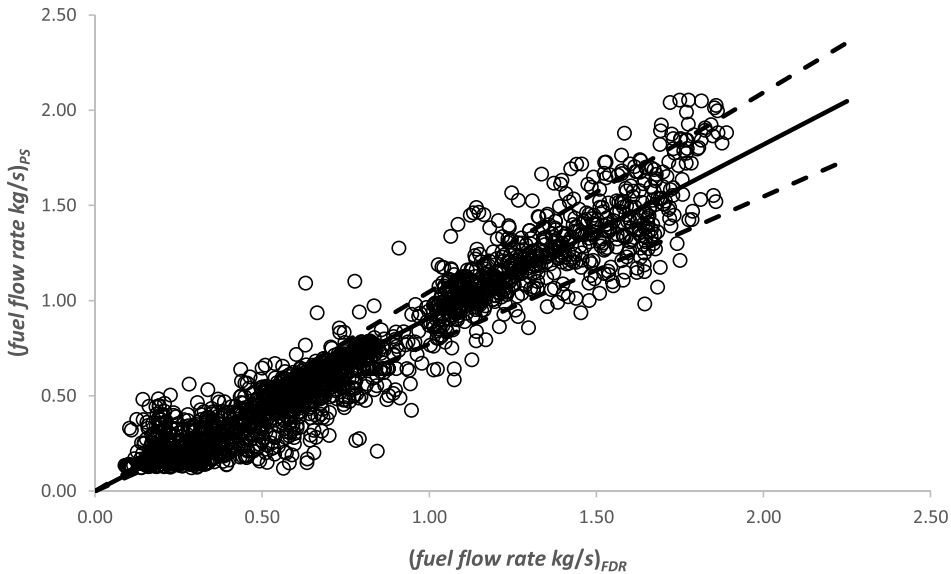
Figure 9. *Comparison between estimates for fuel flow rate and values obtained from the flight data recorder on an Airbus A320-200 aircraft. Data are taken from 20 complete flights $\approx$2,200 points. The solid line shows the mean variation, which has a slope of 0.91 and the dashed lines show the $\pm$ 15% variation.*

10.0 Comparison with flight data recorder information

The type of in-flight information required to test any performance model is commercially sensitive and, consequently, examples rarely appear in the public domain. However, some years ago Swiss International Airlines released a set of flight recorder data (*FRD*) from operations in 2008 and this has been used in a number of studies, e.g. Randle et al. [17], Simone et al. [18] and, more recently, Hall et al. [19]. The aircraft involved are single examples of the Airbus A320-200, A330-200 and A340-300 and the Boeing B757-300, B767-300 and B777-300 types, operating on different routes. There are 885 complete flights covering the North Atlantic, the tropics and the Indian Ocean, with a wide range of operational conditions, masses ranging from empty and to the maximum take-off values and ambient temperatures between $\pm$20 K relative to *ISA*.

The measurement accuracy of the data has been discussed by Vera-Morales and Hall [20], Randle et al. [17] and Simone et al. [18]. They estimate that the fuel flow data are accurate to $\pm$1 %, whilst the estimated accuracies of *FL*, M_∞, and T_∞ to be $\pm$0.3, $\pm$0.01, and $\pm$2K, respectively. In addition, the instantaneous aircraft mass depends upon the input value take-off mass, whose accuracy is not known. The data are also very noisy, exhibiting fluctuations in excess of $\pm$10%. There could be many reasons for this, including errors introduced during data processing, oscillations due to dynamic response to turbulence and other perturbations such as minor pilot, or autopilot, control inputs.

Figures 9–14 show comparisons between the estimates for instantaneous fuel flow rate and the values from the flight data recorder. In each case, 20 complete flights are shown and they have been filtered using the performance boundaries described in Section 5[12]. The results arrange themselves into broad groups representing the climb, cruise and descent phases. It is also clear that, whilst the noise level is significant, the majority of the data fall within $\pm$15% of the mean line.

---

[12]When applying the manoeuvre and the minimum climb rate criteria, the low-speed value of $(C_L)_{mu}/(C_L)_{DO}$ and the value of *TR* from Equation (52) have both been increased by 20%. This reflects the maximum uncertainty in these parameters and minimises the rejection of potentially valid data.
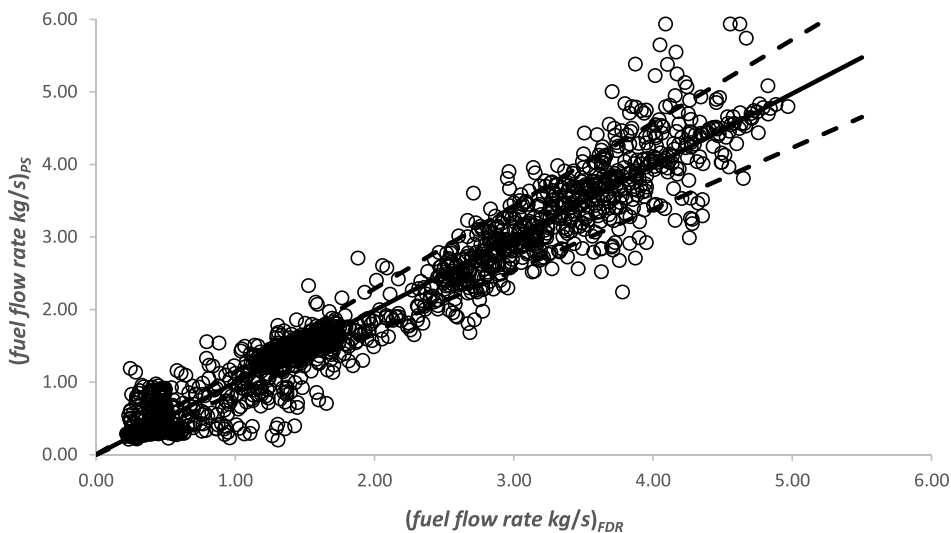
Figure 10. *As for Fig. 9, but for an Airbus A330-200, with ≈2,850 points and a slope of 1.00.*
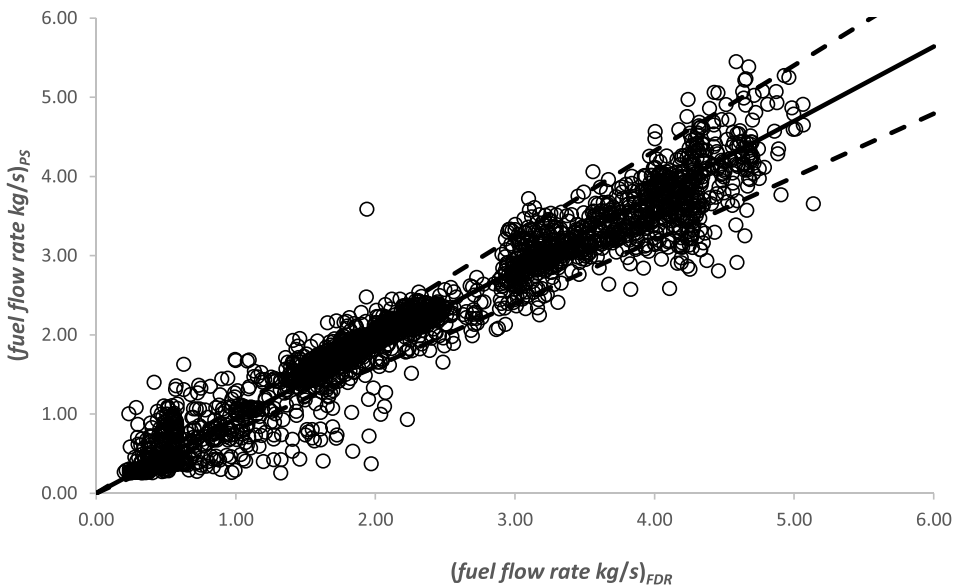
**Figure 11.** *As for Fig. 9, but for an Airbus A340-300, with ≈3,850 points and a slope of 0.94.*

The slope of the mean line depends, primarily, upon a combination of two factors. The first is the accuracy of the model parameter values listed in Tables 1 and 2, whilst the second is the accuracy of the assumed aircraft take-off mass. As can be seen from Equation (2), in steady, straight and level cruise, $(\eta_o L/D)$ is constant and, hence, the fuel flow rate is directly proportional to the aircraft's instantaneous mass. There is a stronger dependency on mass in the climb and a weaker dependency in the descent. Nevertheless, numerical experiments on the data for complete flights show that the slope of the mean line is almost directly proportional to the assumed value of the take-off mass.
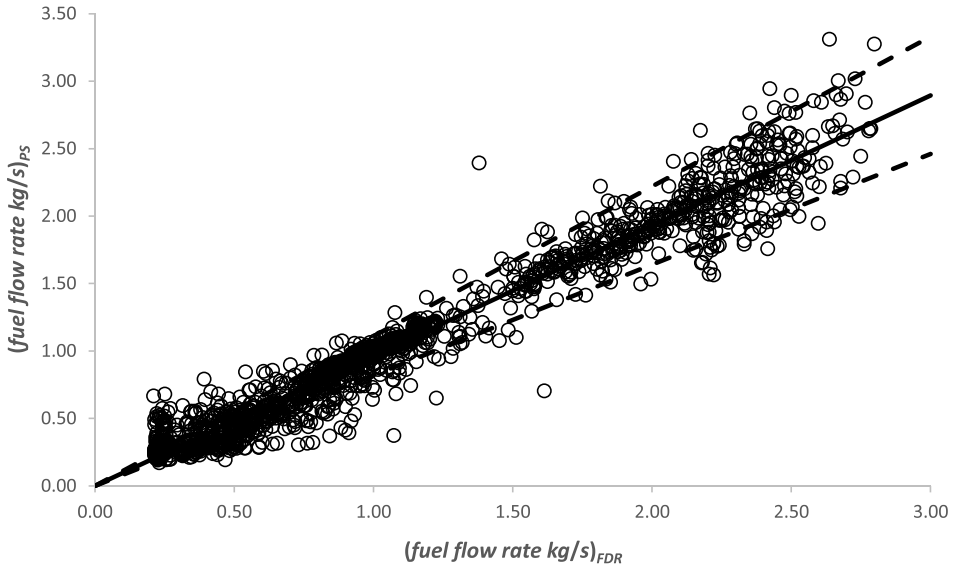
Figure 12. *As for Fig. 9, but for a Boeing B757-300, with $\approx$2,100 points and a slope of 0.97.*
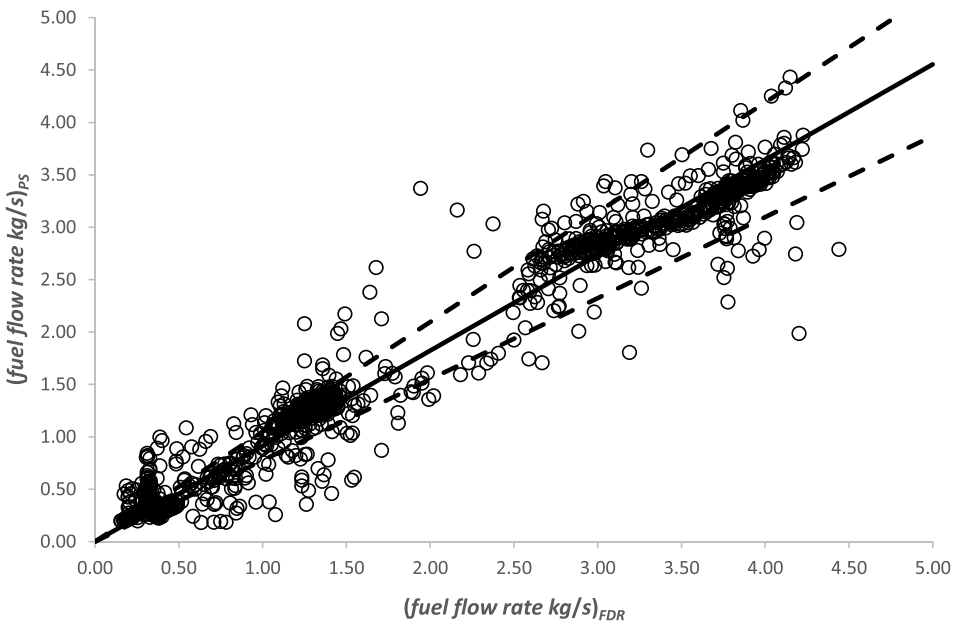
Figure 13. *As for Fig. 9, but for a Boeing B767-300, with $\approx$1,900 points and a slope of 0.91.*

Whilst the *FDR* information includes take-off mass, its origin is unknown and its accuracy does not appear to have been assessed. Take-off mass is an important parameter for aircraft performance. However, in normal operations, aircraft weight is not measured directly before departure. Consequently, the signed-off, take-off mass may not be exactly equal to the true take-off mass. There may be several reasons for this mismatch, for example the passenger weight is estimated and the taxi-out fuel may not all be used prior to take-off.
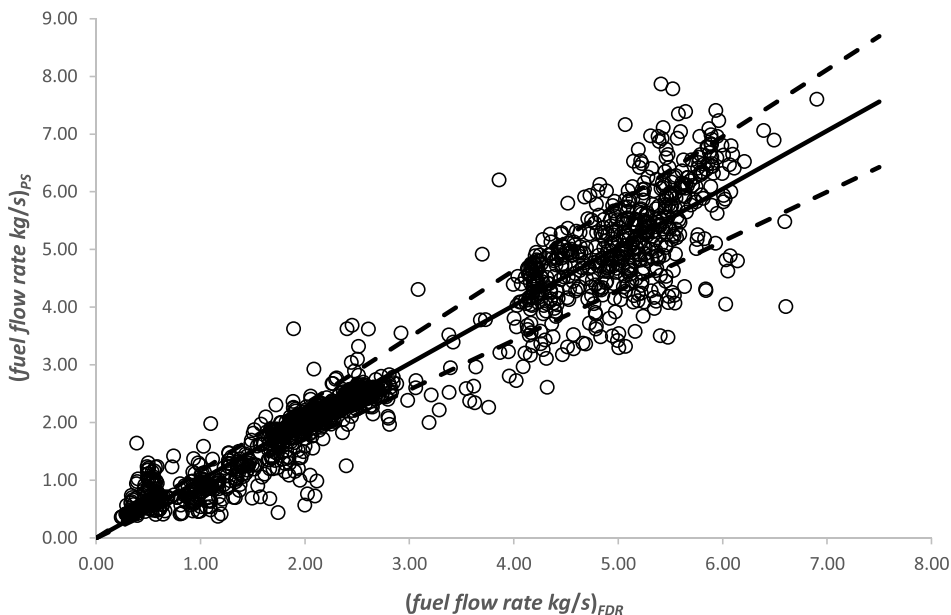
Figure 14. *As for Fig. 9, but for a Boeing B777-300, with ≈2,700 points and a slope of 1.00.*

Notwithstanding the potential uncertainty relating to take-off mass, the overall agreement between the estimates and the FDR values is good, demonstrating that, within reasonable uncertainty bounds, the method works in all phases of flight.

When the estimates for the total amount of fuel used on each flight are compared, the mean deviations relative to the *FDR* values are −10% for the A320, +1% for the A330, −2% for the A340, −1% for the B757, −3% for the B767 and 0% for the B777. Once again, the total fuel used is directly proportional to the assumed take-off mass[13] and so these discrepancies are also due to a combination of errors in the model parameter values and in the assumed take-off mass. Figure 15 shows the comparisons for the total amount of fuel used on each of the 885 flights. The results have been normalised for each aircraft so that deviations from the mean values can be determined. The residual RMS error is found to be less than 2%, with just one point exhibiting an error of more than 10%.

Further improvements in the model will be possible if more flight data, with well characterised accuracy, become available.

11.0 Conclusions

A performance model has been developed for an aircraft in the clean configuration that can be used in climb, cruise, initial descent and holding. It is based upon previously published methods for the estimation of optimum value ($\eta_o L/D$), using a simple relation for the wave drag, and a model for the engine overall efficiency as a function of Mach number and thrust. The method can be used in situations where both the aircraft trajectory and the variation of atmospheric temperature with atmospheric pressure and the wind speed components are fully specified. Such data sets are becoming available to the research community and they will be used to give improved insight into the impact of aviation on the environment.

To provide coverage in all phases of flight, a simplified model of the fuel flow rate in the flight idle mode has been proposed, together with some approximate estimates of the fuel usage during take-off, initial climb and approach and landing. However, since the fuel flow rates in climb and cruise are an

---

[13]As demonstrated in the classic Breguet range equation.
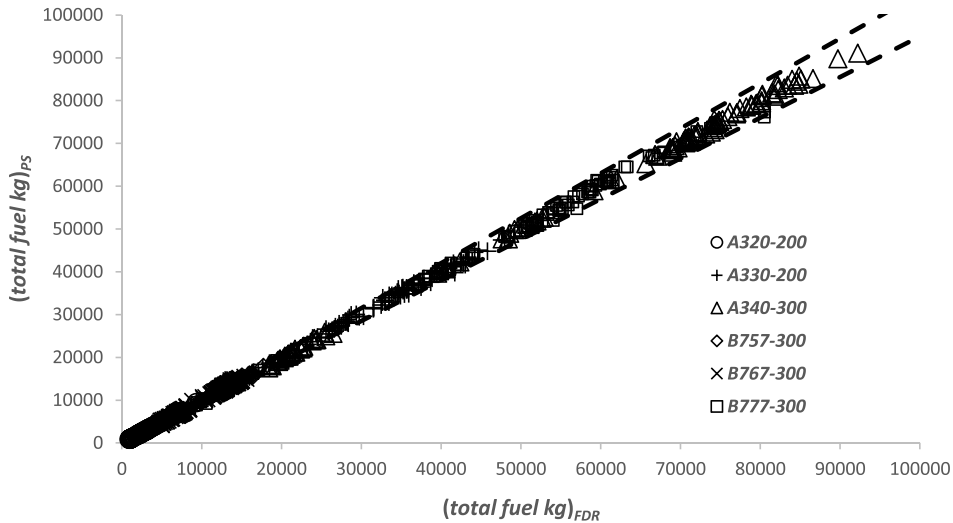
Figure 15. *Comparison of the estimated total trip fuel and the value obtained from the FDR for 885 flights. The data are normalised to remove any differences in the mean values. The dashed lines show the ±5% variation.*

order of magnitude greater than those at flight idle and the amount of fuel used in take-off, initial climb, approach and landing is a small fraction of the total trip fuel, for all but the shortest of flights, the accuracy requirement for these phases is lower than those for climb and cruise.

The operational boundaries imposed by buffet onset and the structural strength constraints of maximum cabin pressure differential and maximum dynamic pressure have been considered and approximate relations have been developed. In addition, since the simplified engine model uses turbine entry temperature as a throttle variable, the service ceiling can also be estimated and its dependence upon the atmospheric static temperature is captured.

When applying the method, a number of airframe and engine specific characteristics must be known. These have already been estimated for a range of aircraft and, as more data has emerged and the method has developed, their accuracy has improved steadily and the number of aircraft in the data base has increased. The latest values for 67 different aircraft and engine combinations are given in tabular form.

Estimates of the instantaneous, fuel flow rates and the total trip fuel per flight have been compared with values from on-board, flight data recorders for six aircraft, covering single and twin aisle types, operating on short, medium and long-range routes. The agreement demonstrates that the method works in all phases of flight. The sensitivity of the estimates to the accuracy of model parameters and potential improvements based upon more test data will be addressed in a subsequent publication.

The method was originally designed as a fully transparent, open-source, emissions estimation method for use by the atmospheric science community to provide information for both individual aircraft and fleets. However, it has now reached a stage where it can be also used by the aircraft performance community and the wider aerospace academic community to obtain general, though approximate, analytic solutions to a range of problems that have previously required highly detailed airframe and engine information and the application of numerical methods. Some of these will be addressed in future work.

References

[1] Schumann, U. On conditions for contrail formation from aircraft exhausts, *Meteorol. Z.*, 1996, **5**, pp 4–23. doi: 10.1127/metz/5/1996/4, https://elib.dlr.de/32128/

[2] Poll, D.I.A. On the relationship between non-optimum operations and fuel requirement for large civil transport aircraft, with reference to environmental impact and contrail avoidance strategy, *Aeronaut. J.*, 2018, **122**, (1258), pp 1827–1870. https://doi.org/10.1017/aer.2018.121

[3] Poll, D.I.A. and Schumann, U. An estimation method for the fuel burn and other performance characteristics of civil transport aircraft in the cruise. Part 1 Fundamental quantities and governing relations for a general atmosphere, *Aeronaut. J.*, 2021, **125**, (1284), pp 257–295. https://doi.org/10.1017/aer.2020.62

[4] Poll, D.I.A. and Schumann, U. An estimation method for the fuel burn and other performance characteristics of civil transport aircraft in the cruise. Part 2 Determining the aircraft's characteristic parameters, *Aeronaut. J.*, 2021, **125**, (1284), pp 296–340. https://doi.org/10.1017/aer.2020.124

[5] Poll, D.I.A. and Schumann, U. On the conditions for absolute minimum fuel burn for turbofan powered, civil transport aircraft and a simple model for wave drag, *Aeronaut. J.*, 2024, **128**, (1324), pp 1071–1103. https://doi.org/10.1017/aer.2024.10

[6] Poll, D.I.A. and Schumann, U. A simple model for the estimation of turbofan engine performance, *Aeronaut. J.*, 2024, **128**, (1330), pp 2725–2753. https://doi.org/10.1017/aer.2024.92

[7] Bower A., Qi Y. and Bazilevs, Y. Introduction to Dynamics and Vibrations, Chapter 3, Section 3.1.4, School of Engineering, Brown University, 2022. https://www.brown.edu/Departments/Engineering/Courses/En4/Notes/particles_eom/particles_eom.htm

[8] Menke, W. and Abbott, D. *Geophysical Theory*, Columbia University Press, 1990, New York, NY, pp 124–126. ISBN 9780231067928.

[9] ICAO. Manual of the ICAO Standard Atmosphere. Document No. 7488/3, ICAO, 3rd Ed, 1993. ISBN 978-92-9249-331-8.

[10] Huang, L.T. and Cummings L.I. A mathematical analysis of the wind triangle problem and an inquiry of true airspeed calculations in supersonic flight, *Int. J. Aviat. Aeronaut. Aerospace*, 2021, **8**, (4). https://doi.org/10.15394/ijaaa.2021.1642

[11] Shevell, R.S. *Fundamentals of Flight*, 2nd Ed, Prentice Hall, 1989, ISBN 0-13-339060-8

[12] Young, T.M. *Performance of the Jet Transport Airplane*, Wiley, 2018, ISBN 9781118384862.

[13] Obert, E. *Aerodynamic Design of Transport Aircraft*, Delft University Press, 2009, ISBN 978-1-58603-970-7.

[14] Jenkinson, L.R., Simpkin, P. and Rhodes, D. *Civil Jet Aircraft Design*, Arnold, 1999, ISBN 0 340 74152 X.

[15] ICAO. Aircraft Engine Emissions Databank EASA, 2018. ICAO Engine Emissions Databank. https://www.easa.europa.eu/easa-and-you/environment/icao-aircraft-engine-emissions-databank

[16] Arrieta, M.de J.G., Botez, R.M. and Lasne, A. An engine deterioration model for predicting fuel consumption in regional aircraft, *Aerospace,* 2024, **11**, (6), 426, pp 1–23. https://doi.org/10.3390/aerospace11060426

[17] Randle, W.E., Hall, C.A. and Vera-Morales, M. Improved range equation based on aircraft flight data, *J. Aircraft*, 2011, **48**, (4), pp 1291–1298. https://doi.org/10.2514/1.C031262

[18] Simone, N.W., Stettler, M.E.J. and Barrett, S.R.H. Rapid estimation of global civil aviation emissions with uncertainty quantification, *Transp. Res. Part D Transp. Environ.*, 2013, **25**, pp 33–41. https://doi.org/10.1016/j.trd.2013.07.001

[19] Hall, C.A., Burnell, S.R. and Deshpande, A.P. Aircraft descent performance based upon flight data, *Aeronaut. J.*, 2021, **125**, (1293), pp 1897–1916. https://doi.org/10.1017/aer.2021.65

[20] Vera-Moreles, M. and Hall, C.A. Modelling performance and emissions from aircraft for the Integrated Modelling Project, *J. Aircraft*, 2010, **47**, (3), pp 812–819. https://doi.org/10.2514/1.44020

Appendix A. The determination of climb rate and the relationship between flight level and the geometric height above sea level

The variation of static pressure, p_∞, with geodetic height, h, in any atmosphere is determined by the hydrostatic equation, where

$$dp_\infty = -\rho_\infty g dh. \tag{A1}$$

Here, g is the local value of the acceleration in the vertical direction due to the combined effects of gravity and centrifugal acceleration. It is a function of both latitude, ϕ, and h and may be expressed as

$$g = \left(\frac{g_{SL}}{(g_{SL})_{ISA}} \right) \left(\frac{g}{g_{SL}} \right), \tag{A2}$$

where $(g_{SL})_{ISA}$ is equal to 9.80665m/s^2 and g_{SL} is the local vertical acceleration at sea level.

According to Newton's law of gravitation,

$$\frac{g}{g_{SL}} = \frac{r^2}{(r+h)^2} \approx 1 - 2\left(\frac{h}{r}\right), \tag{A3}$$

where r is the local geocentric radius at sea level, i.e. the distance from the point $h(0,\phi)$ to the centre of the Earth[14]. Since the Earth is not a perfect sphere, r_E depends upon the latitude and, if it is assumed that the Earth is an ellipsoid,

$$\frac{r}{r_E} \approx \sqrt{\frac{(r_P/r_E)^2}{1 - \left(1 - (r_P/r_E)^2\right)\cos^2(\phi)}}, \tag{A4}$$

where r_E, the equatorial radius, is 6,378.14km and r_P, the polar radius, is 6,356.75km[15]. In addition, the International Gravity Formula (the Somigliana-Pizzetti empirical relation) may be used to give an estimate of the acceleration due to gravity at sea level as a function of latitude, i.e.

$$\left(\frac{g_{SL}}{(g_{SL})_{ISA}}\right) \approx 0.997316 \left(\frac{1 + 0.00193185\sin^2(\phi)}{\sqrt{1 - 0.00669438\sin^2(\phi)}}\right). \tag{A5}$$

From Equation (A1), the rate of climb is related to the rate of change of static pressure such that

$$\frac{1}{(a_{SL})_{ISA}}\frac{dh}{dt} = -\left(\frac{(g_{SL})_{ISA}}{g_{SL}}\right)\left(\frac{g_{SL}}{g}\right)\left(\frac{\mathfrak{R}T_\infty}{(g_{SL}a_{SL})_{ISA}p_\infty}\frac{dp_\infty}{dt}\right). \tag{A6}$$

All the quantities on the right side of this equation are available from the aircraft's air data system.

From Equation (A1), the geodetic height above local sea level in a general atmosphere is given by

$$\int_0^h dh = h = -\int_{p_{SL}}^{p_\infty}\left(\frac{\mathfrak{R}T_\infty}{gp_\infty}\right)dp_\infty. \tag{A7}$$

Since the integrand is a function of h, this is an implicit integral. However, the implicitness may be removed by introducing the geopotential height, H, which is defined in terms of the work required to raise a fixed mass to a height h, i.e.

$$H = \int_0^h \frac{g}{g_{SL}}dh = \int_0^h \frac{r^2}{(r+h)^2}dh = \frac{rh}{(r+h)} \approx \left(1 - \left(\frac{h}{r}\right)\right)h. \tag{A8}$$

Up to the maximum heights likely to be reached by civil transport aircraft, H differs from h by less than 0.25%.

Again, using Equation (A1),

$$H = -\frac{\mathfrak{R}}{g_{SL}}\int_{p_{SL}}^{p_\infty}\left(\frac{T_\infty}{p_\infty}\right)dp_\infty \tag{A9}$$

and, in the special case of the International Standard Atmosphere [9],

$$H_{ISA} = -\frac{\mathfrak{R}}{(g_{SL})_{ISA}}\left(\int_{p_{SL}}^{p_\infty}\left(\frac{T_\infty}{p_\infty}\right)dp_\infty\right)_{ISA}, \tag{A10}$$

where the variation of T_∞, with p_∞ is specified and p_{SL} is equal to 1.01325 bars. Using the results given in reference 9, if (p_∞/p_{SL}) is greater than 0.223363,

$$H_{ISA} = 3.75422\left(\frac{\gamma\mathfrak{R}T_{SL}}{g_{SL}}\right)_{ISA}\left(1 - \left(\frac{p_\infty}{p_{SL}}\right)_{ISA}^{0.190263}\right), \tag{A11}$$

otherwise

$$H_{ISA} = 0.126533\left(\frac{\gamma\mathfrak{R}T_{SL}}{g_{SL}}\right)_{ISA}\left(1 - 4.24436\,ln\left(\frac{p_\infty}{p_{SL}}\right)_{ISA}\right). \tag{A12}$$

In operations, Equations (A11) and (A12) are used to obtain H_{ISA} from the value of p_∞ provided by the air-data system. This barometric equivalent, geopotential altitude is the value of the geopotential height that the aircraft would have if it was operating in the ISA.

---

[14]Strictly speaking, the altitude used in Equation (A3) should be the geocentric height above local sea level and not the geodetic height. However, the difference between the two is very small and can be ignored.

[15]These values are from World Geodetic System (WGS) 1984 Ellipsoidal Gravity Formula.

By definition, flight level, *FL*, has no units and it is numerically equal to H_{ISA} when expressed in units of feet and divided by 100. Hence, if $(p_\infty/(p_{SL})_{ISA})$ is greater than 0.223363,

$$FL = 1454.43 \left(1 - \left(\frac{p_\infty}{(p_{SL})_{ISA}} \right)^{0.190263} \right), \tag{A13}$$

otherwise

$$FL = 49.0202 \left(1 - 4.24436 \ln \left(\frac{p_\infty}{(p_{SL})_{ISA}} \right) \right). \tag{A14}$$

It follows from Equation (A1) that the true rate of climb is given by

$$\frac{1}{(a_{SL})_{ISA}} \frac{dh}{dt} = - \left(\frac{(g_{SL})_{ISA}}{g_{SL}} \right) \left(\frac{g_{SL}}{g} \right) \left(\frac{\Re T_\infty}{a_{SL}g_{SL}} \right)_{ISA} \left(\frac{T_\infty}{(T_\infty)_{ISA}} \right) \left(\frac{1}{p_\infty} \frac{dp_\infty}{dFL} \right) \frac{dFL}{dt}, \tag{A15}$$

which, noting the properties of the *ISA*, if *h* is in metres and *t* is in seconds

$$\frac{dh}{dt} = 30.48 \left(\frac{(g_{SL})_{ISA}}{g_{SL}} \right) \left(\frac{g_{SL}}{g} \right) \left(\frac{T_\infty}{(T_\infty)_{ISA}} \right) \frac{dFL}{dt} \quad \text{(m/s)} . \tag{A16}$$

Since *g* varies with *h*, Equations (A15) and (A16) are still implicit. However, a good estimate is obtained by either setting *h* equal to 30.48(*FL*) or by ignoring the vertical variation of *g* altogether. Greater accuracy can always be achieved by iteration.

Appendix B. Pressure and speed information from the air data system

In-flight values of the freestream total pressure, p_0, total temperature, T_0, and the atmospheric static pressure, p_∞, as a function of time are provided by the aircraft's air data system. The difference between the total and static pressures is known as the impact pressure, p_i, and, using the standard adiabatic and isentropic flow relations, e.g. Shevell [11],

$$p_i = p_0 - p_\infty = p_\infty \left(\left(1 + \frac{(\gamma - 1)}{2} M_\infty^2 \right)^{\frac{\gamma}{(\gamma-1)}} - 1 \right). \tag{B1}$$

Hence, the Mach number is

$$M_\infty = \sqrt{ \frac{2}{(\gamma - 1)} \left(\left(\frac{p_i}{p_\infty} + 1 \right)^{\frac{(\gamma-1)}{\gamma}} - 1 \right) } \tag{B2}$$

and, since the atmospheric static temperature, T_∞, is given by

$$T_\infty = \frac{T_0}{\left(1 + \frac{(\gamma-1)}{2} M_\infty^2 \right)}, \tag{B3}$$

the true airspeed, V_∞, is

$$V_\infty = M_\infty \sqrt{\gamma \Re T_\infty}. \tag{B4}$$

Another speed used in both aircraft performance and design is the calibrated airspeed, V_{CAS}. This is defined as the speed at sea level in the *ISA* that corresponds to a given impact pressure, i.e.

$$p_i = p_0 - p_\infty = (p_{SL})_{ISA} \left(\left(1 + \frac{(\gamma - 1)}{2} \left(\frac{V_{CAS}}{(a_{SL})_{ISA}} \right)^2 \right)^{\frac{\gamma}{(\gamma-1)}} - 1 \right), \tag{B5}$$

or

$$V_{CAS} = (a_{SL})_{ISA} \sqrt{ \frac{2}{(\gamma - 1)} \left(\left(\frac{p_i}{(p_{SL})_{ISA}} + 1 \right)^{\frac{(\gamma-1)}{\gamma}} - 1 \right) }. \tag{B6}$$

The impact pressure is closely related to two other important quantities, namely the dynamic pressure, q_∞, and the equivalent air speed, V_{EAS}. Using the definition of equivalent air speed, series expansion and neglecting terms that are small compared to unity,

$$q_\infty = \frac{\gamma}{2} p_\infty M_\infty^2 = \frac{\gamma}{2} (p_{SL})_{ISA} \left(\frac{V_{EAS}}{(a_{SL})_{ISA}} \right)^2 = \frac{p_i}{f(M_\infty)} \approx \frac{p_i}{\left(1 + \frac{M_\infty^2}{4} + (2-\gamma)\frac{M_\infty^4}{24} \right)}. \tag{B7}$$

This equation may be rearranged to give an approximate relation for Mach number, i.e.

$$M_\infty \approx \sqrt{2 \left(\left(\frac{2}{\gamma} \frac{p_i}{p_\infty} + 1 \right)^{\frac{1}{2}} - 1 \right)} \tag{B8}$$

and, using Equation (B5),

$$\left(\frac{V_{CAS}}{V_{EAS}} \right)^2 = f(M_\infty) \left(1 - \frac{1}{4} \left(f(M_\infty) \left(\frac{V_{EAS}}{(a_{SL})_{ISA}} \right)^2 \right) + \frac{1}{10} \left(f(M_\infty) \left(\frac{V_{EAS}}{(a_{SL})_{ISA}} \right)^2 \right)^2 + \dots \right). \tag{B9}$$

Appendix C. Extension of the relation between normalised engine overall efficiency and normalised thrust to values below 0.3

For values of the normalised thrust coefficient ratio below 0.3, the variation is represented by a 4th order polynomial passing through zero when the thrust coefficient ratio is zero and matching Equation (24) for value, first derivative and second derivative when it is equal to 0.3. Therefore, let

$$\frac{\eta_o}{(\eta_o)_B} = h_0 = H_1 \left(\frac{C_t}{(C_t)_{\eta B}} \right) + H_2 \left(\frac{C_t}{(C_t)_{\eta B}} \right)^2 + H_3 \left(\frac{C_t}{(C_t)_{\eta B}} \right)^3. \tag{C1}$$

Then, for

$$0 \leq \frac{C_t}{(C_t)_{\eta B}} \leq 0.3, \tag{C2}$$

$$H_1 = 6.560 \left(1 + 0.8244 \Sigma \right), \tag{C3}$$

$$H_2 = -19.43 \left(1 + 1.053 \Sigma \right) \tag{C4}$$

and

$$H_3 = 21.11 \left(1 + 1.063 \Sigma \right). \tag{C5}$$

Appendix D. Approximate 1.3g manoeuvre boundary

Using data taken from the *FCOM* of a typical jet transport aircraft, an estimate of the 1.3g manoeuvre boundary for the aircraft in the "clean" condition and having the centre of gravity at 35% of the mean aerodynamic chord is given by

$$\frac{(C_L)_{mu}}{(C_L)_{DO}} \approx \left(\frac{(C_L)_{mu}}{(C_L)_{DO}} \right)_{LS} \left(1.00 + 0.089 \left(\frac{M_\infty}{M_{DO}} \right) - 0.603 \left(\frac{M_\infty}{M_{DO}} \right)^2 \right), \tag{D1}$$

for

$$0 \leq \frac{M_\infty}{M_{DO}} < 0.7, \tag{D2}$$

and

$$\frac{(C_L)_{mu}}{(C_L)_{DO}} \approx \left(\frac{(C_L)_{mu}}{(C_L)_{DO}}\right)_{LS} \left(7.373 - 23.479\left(\frac{M_\infty}{M_{DO}}\right) + 27.713\left(\frac{M_\infty}{M_{DO}}\right)^2 - 10.935\left(\frac{M_\infty}{M_{DO}}\right)^3\right), \quad \text{(D3)}$$

for

$$0.7 \leq \frac{M_\infty}{M_{DO}} \leq \frac{M_{MO}}{M_{DO}}, \quad \text{(D4)}$$

where, M_{MO} is the maximum permitted operational Mach number and

$$\left(\frac{(C_L)_{mu}}{(C_L)_{DO}}\right)_{LS} = 1.8 \pm 0.4. \quad \text{(D5)}$$

This boundary should only be applied when the aircraft is above 3,000 feet, since, below this altitude the aircraft is unlikely to be in the clean condition.

Appendix E. Approximate estimate of the Service Ceiling

From Equations (8) and (9), assuming small angles and neglecting small terms,

$$\frac{dh}{dt} \approx V_\infty \frac{(n.F_n - D)}{mg_n} = M_\infty a_\infty \frac{(C_T - Cd)}{C_L}. \quad \text{(E1)}$$

At the aircraft's service ceiling, the engines are operating at their maximum continuous climb rating, $(TET)_{MCC}$, and the rate of climb is equal to 300 feet/min. The corresponding lift coefficient, $(C_L)_{SC}$ is obtained by using the aircraft drag polar given in Equation (39) and rearranging (E1) to give

$$K\,(C_L)^2_{SC} + \frac{0.00516}{M_\infty}\left(\frac{(T_{TP})_{ISA}}{T_\infty}\right)^{1/2}(C_L)_{SC} - ((C_T)_{MCC} - (Cd_0 + Cd_w)) = 0. \quad \text{(E2)}$$

As shown in Ref. (6), net thrust is governed by the throttle parameter, T_R, such that

$$\frac{C_t}{(C_t)_{\eta B}} = \frac{C_T}{(C_T)_{\eta B}} = h_4 \approx f(T_R) \approx 1 + 2.50\,(T_R - 1) \quad \text{(E3)}$$

where

$$T_R = \frac{TET/(T_0)_\infty}{(TET/(T_0)_\infty)_{\eta B}} \approx \left(\frac{1}{TR_{EC}}\right)\frac{(TET/T_\infty)}{\left(1 - 0.53(M_\infty - M_{EC})^2\right)\left(1 + 0.2M_\infty^2\right)}, \quad \text{(E4)}$$

and

$$\left(\frac{T_0}{T}\right)_\infty = 1 + \left(\frac{\gamma - 1}{2}\right)M_\infty^2. \quad \text{(E5)}$$

Here, TR_{EC} and M_{EC} are constants, whilst $(C_T)_{\eta B}$ is given by Equation (28). Hence, for any combination of speed and altitude, $(TET)_{MCC}$, ambient air temperature and Mach number determine the value of the maximum available thrust coefficient, $(C_T)_{MCC}$. Using Equations (28), (E3) and (E4),

$$(C_T)_{MCC} \approx (C_T)_{DO}\left(\frac{1 + 0.55M_\infty}{1 + 0.55M_{DO}}\right)\left(\frac{M_{DO}}{M_\infty}\right)^2\left(\left(\frac{2.5}{TR_{EC}}\right)\frac{((TET)_{MCC}/(T_0)_\infty)}{\left(1 - 0.53(M_\infty - M_{EC})^2\right)} - 1.5\right). \quad \text{(E6)}$$

Therefore, in a given atmosphere, the maximum available thrust coefficient is a function of Mach number and FL only. Estimates for TR_{EC}, M_{EC} and TET_{MCC} are listed in Table 1.

Similarly, the drag coefficient of an aircraft of given weight in straight and level flight is a function of Mach number and FL only. Therefore, the corresponding values for Cd_0 and Cd_w are obtained using the method given in Section 4. With all the parameters specified, the value $(C_L)_{SC}$ follows from an iterative solution of Equation (E2) and examples of the full solution are given in Figs 6 and 7. The results show

that the flight level at the service ceiling is not particularly sensitive to the Mach number. Therefore, a reasonable estimate is obtained by assuming that the Mach number is equal to the M_{DO}.

Neglecting terms that are small compared to unity, the approximate solution to Equation (E2) is

$$(C_L)_{SC} \approx \left(\frac{(C_T)_{MCC} - (Cd_0 + Cd_w)}{K} \right)^{1/2} - \frac{0.00516}{2KM_{DO}} \left(\frac{(T_{TP})_{ISA}}{T_\infty} \right)^{1/2}. \tag{E7}$$

From Equation (E6), also neglecting quantities that are small compared to unity,

$$(C_T)_{MCC} \approx (C_T)_{DO} \left(\left(\frac{2.5}{TR_{EC} \left(1 + 0.2M_{DO}^2 \right)} \right) \left(\frac{(TET)_{MCC}}{T_\infty} \right) - 1.5 \right). \tag{E8}$$

In addition, since Cd_0 and Cd_w are only weakly dependent upon C_L and $(Cd)_{DO}$ is equal to $(C_T)_{DO}$,

$$(Cd_0 + Cd_w)_{M_{DO}} \approx (Cd_0 + Cd_w)_{DO} = (C_T)_{DO} \left(1 - \left(\frac{K(C_L)_{DO}^2}{(Cd)_{DO}} \right) \right). \tag{E9}$$

Hence,

$$\frac{(C_L)_{SC}}{(C_L)_{DO}} \approx \left(c_1 \left(\frac{(TET)_{MCC}}{T_\infty} \right) + c_2 \right)^{1/2} - c_3 \left(\frac{(T_{TP})_{ISA}}{T_\infty} \right)^{1/2} \tag{E10}$$

where

$$c_1 = \frac{2.5(C_T)_{DO}}{K.TR_{EC} \left(1 + 0.2M_{DO}^2 \right)}, \tag{E11}$$

$$c_2 = \left(\frac{K(C_L)_{DO}^2}{(Cd)_{DO}} \right) - \frac{(C_T)_{DO}}{K}, \tag{E12}$$

and

$$c_3 = \frac{0.00258}{K(C_L)_{DO}M_{DO}}. \tag{E13}$$

All the parameters in Equation (E10), except T_∞, are given in Tables 1 and 2.